

# Influence of Ocean Alkalinity Enhancement with Olivine or Steel Slag on a Coastal Plankton Community in Tasmania

Jiaying A. Guo<sup>1,2</sup>, Robert F. Strzepek<sup>2</sup>, Kerrie M. Swadling<sup>1,2</sup>, Ashley T. Townsend<sup>3</sup>, Lennart T. Bach<sup>1</sup>

<sup>1</sup>Institute for Marine and Antarctic Studies, University of Tasmania, Hobart, Tasmania, 7000 Australia

<sup>2</sup>Australian Antarctic Program Partnership (AAPP), Institute for Marine and Antarctic Studies, University of Tasmania, Hobart, Tasmania, 7000 Australia

<sup>3</sup>Central Science Laboratory, University of Tasmania, Sandy Bay, Tasmania, 7005 Australia

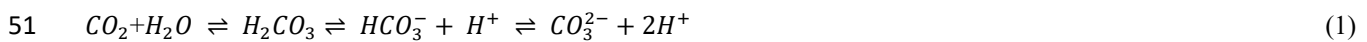
Correspondence to: Jiaying A. Guo (Jiaying.guo@utas.edu.au)

**Abstract.** Ocean alkalinity enhancement (OAE) aims to increase atmospheric CO<sub>2</sub> sequestration in the oceans through the acceleration of chemical rock weathering. This could be achieved by grinding rocks containing alkaline minerals and adding the rock powder to the surface ocean where it dissolves and chemically locks CO<sub>2</sub> in seawater as bicarbonate. However, CO<sub>2</sub> sequestration during dissolution coincides with the release of potentially bio-active chemicals and may induce side effects. Here, we used 53 L microcosms to test how coastal plankton communities from Tasmania respond to OAE with olivine (mainly Mg<sub>2</sub>SiO<sub>4</sub>) or steel slag (mainly CaO and Ca(OH)<sub>2</sub>) as alkalinity sources. Three microcosms were left unperturbed and served as a control, three were enriched with olivine powder (1.9 g L<sup>-1</sup>), and three with steel slag powder (0.038 g L<sup>-1</sup>). Olivine and steel slag powders were of similar grain size. Olivine was added in a higher amount than the steel slag with the aim to compensate for the lower efficiency of olivine to deliver alkalinity over the 3-week experiment. Phytoplankton and zooplankton community responses as well as some biogeochemical parameters were monitored. Olivine and steel slag additions increased total alkalinity by 29 μmol kg<sup>-1</sup> and 361 μmol kg<sup>-1</sup> respectively, which corresponds to a theoretical increase of 0.9 % and 14.8 % of the seawater storage capacity for atmospheric CO<sub>2</sub>. Olivine and steel slag released silicate nutrients into the seawater, but steel slag released considerably more and also significant amounts of phosphate. After 21 days, no significant difference was found in dissolved iron concentrations (>100 nmol L<sup>-1</sup>) in the treatments and the control. The slag addition increased dissolved manganese concentrations (771 nmol L<sup>-1</sup>), while olivine increased dissolved nickel concentrations (37 nmol L<sup>-1</sup>). There was no significant difference in total chlorophyll *a* concentrations between the treatments and the control, likely due to nitrogen limitation of the phytoplankton community. However, flow cytometry results indicated an increase in the cellular abundance of several smaller (~<20 μm) phytoplankton groups in the olivine treatment. The abundance of larger phytoplankton (~>20 μm) decreased much more in the control than in the treatments after day 10. Furthermore, the maximum quantum yields of photosystem II (F<sub>v</sub>/F<sub>m</sub>) were higher in slag and olivine treatments, suggesting that mineral additions increased photosynthetic performance. The zooplankton community composition was also affected with the most notable changes being observed in the dinoflagellate *Noctiluca scintillans* and the appendicularian *Oikopleura* sp. in the olivine treatment. Overall, steel slag is much more efficient for CO<sub>2</sub> removal with OAE than olivine and appears to induce less change in the plankton community when relating the CO<sub>2</sub> removal potential to the level of environmental impact that was observed here.

## 36 1 Introduction

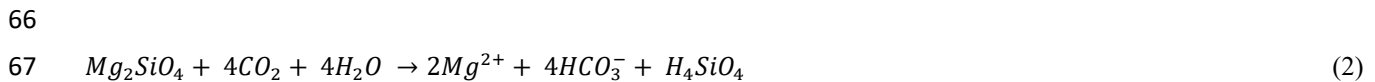
37 Keeping global warming below 2 °C requires immediate emissions reduction. Additionally, between 450-1100 Gigatonnes  
38 of carbon dioxide (CO<sub>2</sub>) need to be removed from the atmosphere by 2100 (Smith et al., 2023). This could be achieved  
39 with a portfolio of terrestrial and marine Carbon Dioxide Removal (CDR) methods. Ocean alkalinity enhancement (OAE)  
40 is a marine CDR method that could theoretically contribute significantly to the global CDR portfolio (Ilyina et al., 2013;  
41 Feng et al., 2017; Lenton et al., 2018).

42  
43 Alkalinity is generated naturally when rock weathers and it has control on the ocean's chemical capacity to store CO<sub>2</sub>  
44 (Schuiling and Krijgsman, 2006). Natural rock weathering is currently responsible for about 0.5 Gt of atmospheric CO<sub>2</sub>  
45 sequestration every year (Renforth and Henderson, 2017). The idea behind OAE is to accelerate natural rock weathering  
46 by extracting calcium- or magnesium-rich rocks, such as olivine, pulverizing them, and spreading them onto the sea surface  
47 to increase chemical weathering rates (Hartmann et al., 2013). The weathering (i.e., dissolution) of these alkaline minerals  
48 will consume protons (H<sup>+</sup>), which shifts the carbonate chemistry equilibrium in seawater from CO<sub>2</sub> towards increasing  
49 bicarbonate (HCO<sub>3</sub><sup>-</sup>) and carbonate ion (CO<sub>3</sub><sup>2-</sup>) concentrations:



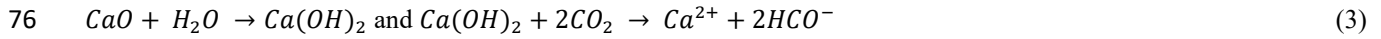
52  
53 thereby making new space for atmospheric CO<sub>2</sub> to be dissolved in seawater and permanently stored. Previous model studies  
54 have shown that OAE can mitigate climate change significantly by increasing the oceanic uptake of CO<sub>2</sub> from the  
55 atmosphere (Kohler et al., 2010; Paquay and Zeebe, 2013; Keller et al., 2014; Lenton et al., 2018). For example, the study  
56 by Burt et al. (2021) suggested that the total global mean dissolved inorganic carbon (DIC) inventories would increase by  
57 156 GtC after total alkalinity is enhanced at a rate of 0.25 Pmol year<sup>-1</sup> in 75-year simulations.

58  
59 There are a variety of alkaline minerals that could be used for OAE. A widely considered naturally occurring mineral is  
60 forsterite, a (Mg<sub>2</sub>SiO<sub>4</sub>)-rich olivine. This type of olivine is abundant in ultramafic rock such as dunite, constituting at least  
61 88 % of the rock composition (Ackerman et al., 2009; Su et al., 2016). Olivine occurs in the Earth's crust but is more  
62 abundant in the upper mantle. There are at least several billion tons of olivine resources on Earth (Caserini et al., 2022).  
63 However, the extraction of olivine in 2017 was only around 8.4 Mt year<sup>-1</sup> (Reichl et al., 2018), which is about two orders  
64 of magnitude below the mass needed for climate-relevant OAE with olivine (Caserini et al., 2022). The net reaction for  
65 CO<sub>2</sub> sequestration with Mg<sub>2</sub>SiO<sub>4</sub> is:



68  
69 Another potential OAE source material is steel slag (Renforth, 2019), a by-product of steel manufacturing. During steel  
70 manufacturing, high-purity calcium oxide (CaO) is used to improve the quality of the steel through accumulation of  
71 unwanted materials such as sulphur and phosphorus. Steel slag mainly contains CaO, SiO<sub>2</sub>, Al<sub>2</sub>O<sub>3</sub>, Fe<sub>2</sub>O<sub>3</sub>, MgO, and MnO  
72 (Kourounis et al., 2007), and the chemical composition can vary depending on the manufacturing process (Wang et al.,  
73 2011). Due to the presence of CaO and potentially other alkaline components, steel slag can increase alkalinity when  
74 dissolved in seawater. The chemical reaction for CO<sub>2</sub> sequestration with CaO is:

75



77

78 Some of the steel slag that is produced during steel manufacturing is further used (e.g., for road construction and civil  
79 engineering) but in some countries like China, 70.5 % of steel slag is left unused and stored in dumps (Guo et al., 2018).  
80 In 2016, more than 300 million tons of steel slag was not used effectively, thereby occupying the land and raising  
81 environmental concerns (Guo et al., 2018). The effective alkaline composition, availability, and relatively low cost of the  
82 raw materials make olivine and steel slag potential source materials for OAE.

83

84 To assess whether OAE is viable, it needs to be understood how its application may affect marine biota such as plankton  
85 and the biogeochemical fluxes they drive. Some data on the effects of OAE with sodium hydroxide (NaOH) on plankton  
86 communities have recently been published (Ferderer et al., 2022; Subhas et al., 2022), but to the best of our knowledge, no  
87 such data are available for olivine- and/or slag-based OAE. Chemical perturbations via olivine and slag should be like  
88 those by NaOH in that they increase seawater pH and shift the carbonate chemistry equilibrium (see Eq. 1). However, there  
89 would be additional chemical perturbations because minerals contain a variety of potentially bioactive elements that are  
90 released into the environment when they dissolve in seawater (Bach et al., 2019). One particular concern is that natural and  
91 anthropogenic minerals such as olivine and steel slag are rich in bioactive metals that are usually scarce in the ocean, such  
92 as iron (Fe), copper (Cu), nickel (Ni), manganese (Mn), zinc (Zn), cadmium (Cd), and chromium (Cr). Many of these trace  
93 metals are essential micronutrients for phytoplankton growth (Sunda, 2000; Sunda, 2012), such as being co-factors for  
94 various metalloenzymes (summarized by Twining and Baines, 2013). It is possible that the addition of alkaline minerals  
95 may benefit phytoplankton by providing trace metals currently limiting phytoplankton growth (Falkowski, 1994; Basu and  
96 Mackey, 2018). For instance, the addition of Fe is well known to stimulate phytoplankton blooms in those vast ocean  
97 regions where Fe levels limit growth (Boyd et al., 2007; Moore et al., 2013). However, some trace metals can also inhibit  
98 phytoplankton growth, and different phytoplankton species have different requirements and tolerances for trace metals  
99 (Sunda, 2012) so the addition of trace metals via OAE may change phytoplankton community composition.

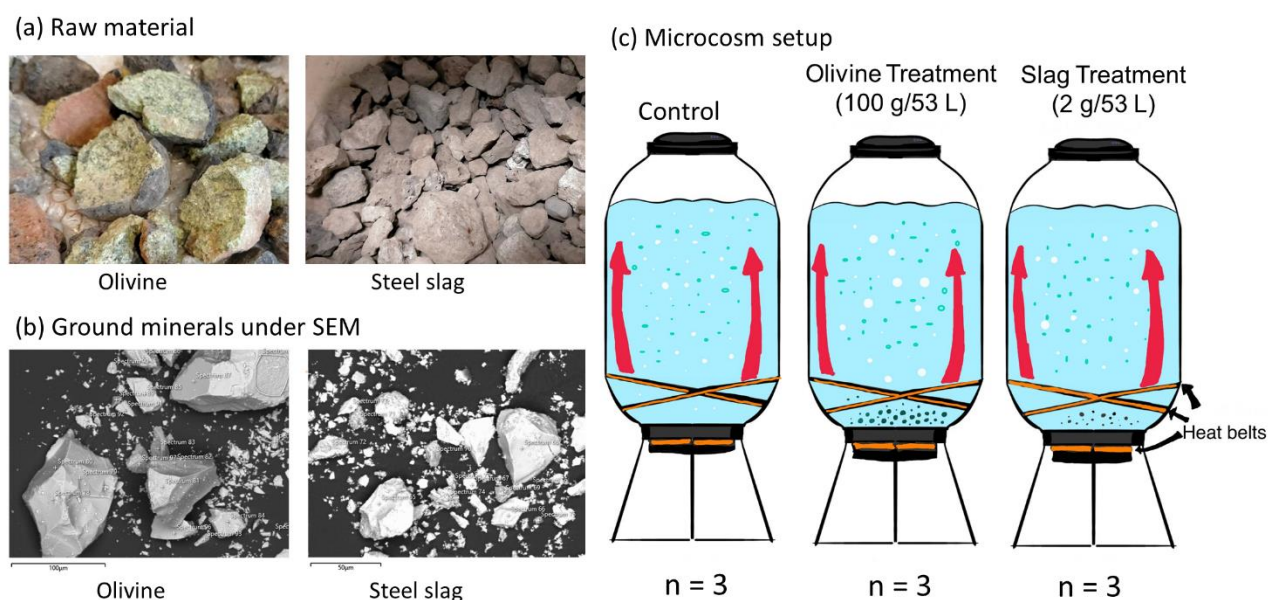
100

101 Here, we describe a microcosm experiment with coastal Tasmanian plankton communities that was used to investigate: (1)  
102 how effectively OAE via the application of finely ground olivine and steel slag could sequester atmospheric CO<sub>2</sub>, and (2)  
103 if/how olivine and steel slag additions affect various components of the plankton community.

104

105 **2 Methodology**

106 **2.1 Microcosm setup**



107

108 **Fig. 1.** Experimental design and alkalinity sources. (a) Raw materials used as alkalinity sources: olivine (left) and steel slag (right).  
109 Olivine and steel slag were originally larger than 20 mm. (b) Ground minerals observed with a scanning electron microscope (SEM). (c)  
110 Microcosm setup: each microcosm enclosed ~ 53 L of surface seawater with natural plankton communities. Olivine and steel slag  
111 treatments and the control were kept in a temperature-controlled room and two heat belts were attached to the bottom of each microcosm  
112 to create convective circulation.

113

114 We used nine 53 L transparent Kegland® Fermzilla conical unitank fermenters (polyethylene terephthalate) (Fig. 1) as  
115 microcosms to incubate natural plankton communities. All microcosms were prewashed with hydrochloric acid (10 % v/v)  
116 and rinsed five times with 18.2 MΩ Milli-Q water. Seawater with coastal plankton communities was collected at Battery  
117 Point, Tasmania (42.892°S, 147.337°E) within 2 hours by lowering the microcosms into the ocean with a crane and filling  
118 them in a manner similar to a Niskin bottle, as described in detail in Ferderer et al. (2022). A sieve with a mesh size of 2  
119 mm was attached to the top and bottom of the microcosms during filling to avoid the entrapment of large and patchily  
120 distributed organisms in the microcosms. The enclosed seawater weight was initially between 52.35-54.70 kg. After  
121 seawater collection, filled microcosms were immediately transported back to the Institute for Marine and Antarctic Studies  
122 (University of Tasmania) on a truck and transferred within 75 min into a temperature-controlled room set to 7.5-8 °C. Two  
123 heat belts were attached to the bottom of each microcosm to induce a convective mixing current (Ferderer et al., 2022).  
124 Seawater temperature inside the microcosms was about 13.5 °C due to the heating effects of the heat belts and was the  
125 same as the sampled region. LED light strips were used to provide an average light intensity of 236  $\mu\text{mol photons m}^{-2} \text{s}^{-1}$   
126 (ranging from 208 to 267  $\mu\text{mol photons m}^{-2} \text{s}^{-1}$ ) with a daily light-dark cycle of 10:14 hours. The light intensity was the  
127 average light intensity in each microcosm measured with a LICOR light meter at 0.15 m depth within the microcosm.  
128 Microcosms positioned in the temperature-controlled room were shuffled anti-clockwise every day to ensure similar light

129 intensity for each microcosm throughout the experiment. Treatments were established 24 hours after collecting the seawater.  
130 The total alkalinity released per amount of mineral powder added was much higher for the slag powder than the olivine  
131 powder in our preliminary test trials. So, three microcosms were enriched with 100 g of olivine powder, three microcosms  
132 with 2 g of steel slag powder, while the remaining three microcosms were left unperturbed and served as controls.

133

134

## 135 **2.2 Preparation of olivine and steel slag powder**

136 The olivine rocks were provided by Moyne Shire Council who sourced the mineral from a quarry in Mortlake, Victoria,  
137 Australia. The Basic Oxygen Slag (hereafter referred to as “slag”) was provided by Bradley Mansell who sourced the  
138 material from Liberty Primary Steel Whyalla Steelworks in Whyalla, South Australia, Australia. Upon delivery, the olivine  
139 rocks were 40-80 mm in diameter, and slag aggregates were 20-50 mm in diameter. These were crushed to smaller than 10  
140 mm pieces using a hydraulic crusher. The crushed material was further ground with a ring mill with a chrome milling pot.  
141 Afterwards, finely-ground samples were sieved to get samples with 150 ~ 250  $\mu\text{m}$  grain size. The sieved olivine and slag  
142 grains were inspected for their appearance and elemental composition using a Hitachi SU-70 analytical field emission  
143 scanning electron microscope (SEM), and energy dispersive spectrometers (Central Science Laboratory (CSL), University  
144 of Tasmania). Grain size spectra were determined with a Sympatec QICPIC particle size analyser LIXCELL (CSL,  
145 University of Tasmania).

146

## 147 **2.3 Seawater sampling**

148 Seawater was transferred with a peristaltic pump from the microcosms at a depth of about 0.15 m into 1 L acid-washed  
149 sampling bottles (LDPE) using an acid-washed silicon tube. Seawater in these bottles was then subsampled for dissolved  
150 trace metal samples, filtrations, Fast Repetition Rate fluorometry (FRRf), and flow cytometry analysis. Samples for  
151 nutrients and total alkalinity (TA) were transferred using the same pump but through a silicone tube into 80 mL HDPE  
152 bottles. Total alkalinity and macronutrient samples were filtered during this process through a 0.2  $\mu\text{m}$  nylon filter attached  
153 to the silicone tube to remove all particles and organisms  $> 0.2 \mu\text{m}$ .

154

## 155 **2.4 Salinity, nutrients, carbonate chemistry, and trace metal analysis**

156 Salinity was measured before and at the end of the experiment using a HACH HQ40d portable meter. The  $\text{pH}_T$  (total scale)  
157 and temperatures were measured daily (2-3 hours after the onset of the light period) using a pH meter (914  
158 pH/Conductometer Metrohm). We recorded voltages and temperature from the pH meter and calibrated the  $\text{pH}_T$  at original  
159 temperature at sampled time using the certified reference material (CRM) Tris buffer following the method described in  
160 SOP6a by Dickson et al. (2007). Briefly, the standard buffer’s pH and voltage at different temperature gradients were  
161 recorded, and temperature vs. voltage polynomial regression data were generated for calculating calibrated pH values ( $\text{pH}_T$ )  
162 (refer to Eq. 3 in SOP6a of Dickson et al. (2007)). The regression could then be used to obtain a CRM pH value for each  
163 temperature and to calibrate the pH measured in the microcosms to the total pH scale.

164

165 Total alkalinity was sampled every four days. It was measured in duplicate using a Metrohm 862 Compact Titrosampler  
166 coupled with an Aquatrode Plus with PT1000 temperature sensor following the SOP3b open-cell titration protocol  
167 described in Dickson et al. (2007). Filtered TA samples were stored at 8 °C for a maximum of 23 days before measurement.  
168 Titration curves were evaluated using the “calculate” script within PyCO2sys by Humphreys et al. (2022). The carbon  
169 chemistry equilibrium was calculated with the R package “seacarb” Gattuso et al. (2023) from  $pH_T$ , TA, phosphate, silicate,  
170 temperature, and salinities using stoichiometric equilibrium constants from Lueker et al. (2000). Dissolved macronutrients  
171 were measured every second day using standard spectrophotometric methods developed by Hansen and Koroleff (1999)  
172 on the day the samples were taken from the microcosms.

173

174 Dissolved trace metal concentrations were measured four times during the experiment: a few hours before olivine and slag  
175 were added, a few hours after these minerals were added on day 2, near the middle of the experiment on day 13, and at the  
176 end of the experiment on day 22. Sixty mL of seawater was collected using an acid-washed 60 mL syringe, and the seawater  
177 was filtered through 25 mm diameter 0.2  $\mu\text{m}$  pore size polycarbonate filters. Unfortunately, we did not notice that 0.2  $\mu\text{m}$   
178 pore size nylon filters (acid washed) were used during sampling on days 1 and 2 so we refiltered these seawater samples  
179 again using 0.2  $\mu\text{m}$  pore size polycarbonate filters after one month. All seawater samples were diluted approximately 20-  
180 fold by weight using Milli-Q water (18.2  $\text{M}\Omega\cdot\text{cm}$  grade) and acidified using 1 % ultrapure HCl. These samples were  
181 analysed using Sector Field Inductively Coupled Plasma Mass Spectrometry (SF-ICP-MS) employing multiple resolution  
182 settings to overcome major spectral interferences. Due to the presence of abundant major metal ions in our samples, such  
183 as Na and Mg, natural open-ocean seawater from the Southern Ocean with very low trace metal concentrations was diluted  
184 20 times with Milli-Q water and used as a representative blank. The same Southern Ocean seawater was enriched with  
185 different gradients of trace metal standards to calculate the samples’ trace metal concentrations. Five of the total 36 samples  
186 had abnormal trace metal concentrations, and 2 of them were from day 1. We considered values as outliers using the  
187 interquartile range (IQR) criterion on pre-addition data, and if values are more than 10 times higher than replicates, they  
188 are also considered as outliers. These samples containing outliers were excluded from the data analysis (Table S1.). The  
189 major likely source of these metal contaminations is sampling in the temperature control room, where precautions were  
190 insufficiently implemented.

191

## 192 **2.5 Particulate matter and plankton community analysis**

193 Chlorophyll *a* was sampled every second day by filtering the seawater through glass fibre filters (GF/F, pore size = 0.7  $\mu\text{m}$ ,  
194 diameter = 25 mm), and filters were stored in 15 mL polypropylene tubes wrapped with aluminium foil and stored at -80 °C  
195 for 50-70 days before measurement. Each filter was immersed in 10 mL 100 % methanol for 18-20 h to extract chlorophyll  
196 from phytoplankton and these samples were analysed on a Turner fluorometer (Model 10-AU) following the method  
197 described by Evans et al. (1987).

198

199 Phytoplankton flow cytometry samples were fixed with 40  $\mu\text{L}$  of a mixture of formaldehyde-hexamine (18 %:10 % v/w)  
200 added to 1400  $\mu\text{L}$  of seawater sample. All bacteria samples (700  $\mu\text{L}$ ) were fixed with 14  $\mu\text{L}$  glutaraldehyde (Electron-  
201 microscope grade, 25 %). After mixing samples with fixatives, samples were stored for 25 minutes at 10 °C, then flash-  
202 frozen in liquid nitrogen, and stored at -80 °C until measurement 83-86 days later. Directly before the measurement,  
203 samples were thawed at 37 °C. Bacteria samples were stained with SYBR green I (diluted in dimethylsulfoxide) at a final

204 ratio of 1:10000 (SYBR Green I: sample).

205

206 A Cytex Aurora flow cytometer (Cytex Biosciences) was used to quantify the abundance of fluorescing particles such as  
207 phytoplankton or stained bacteria. Phytoplankton groups were distinguished based on their fluorescence signal intensity of  
208 different laser excitation/emission wavelength combinations and forward scatter (FSC). The yellow-green laser (centre  
209 wavelength: 577 nm), in combination with FSC signal strength, was used to separate cyanobacteria and cryptophytes from  
210 other phytoplankton. The violet laser (centre wavelength: 664 nm) in combination with FSC was used to distinguish  
211 picoeukaryotes, nanoeukaryotes, and microphytoplankton. The blue laser (centre wavelength: 508 nm) in combination with  
212 FSC was used to distinguish bacteria from other living (i.e., DNA-containing) particles (Fig. S. 1).

213

214 The biovolume of each classified flow cytometry phytoplankton type was calculated using the equation:

215

$$216 \text{ Biovolume} = \text{Cell number count} \times \left(\frac{\text{FSC}}{10248}\right)^{2.14} \quad (4)$$

217

218 where biovolume is the biovolume of the phytoplankton ( $\mu\text{m}^3$ ), cell number is the cell count per mL of sample, and the  
219 FSC is the forward scatter signal value from the flow cytometry. This equation is calculated based on the relationship  
220 between biovolume and FSC for different phytoplankton species (Selfe, 2022). The biovolume of each phytoplankton type  
221 was then divided by the total biovolume of all phytoplankton type to calculate the biovolume proportion of each  
222 phytoplankton type (Biovolume prop.). This derived value was used to estimate the phytoplankton composition in each  
223 microcosm.

224

225 Phytoplankton photosynthetic performance was estimated from the rapid light curves measured with an FRRf (FastOcean  
226 Sensor FRRf3, Chelsea Instruments Group) every second day following the protocol adapted from Schallenberg et al.  
227 (2020). Samples were kept in the dark for 20 minutes before the measurement and then added to the FRR fluorometry  
228 cuvette, which was temperature-controlled at 13.5 °C. Filtered natural seawater was used for blank correction. A channel  
229 with three light wavelengths (450, 530, and 624 nm) was used in each acquisition sequence. At least 10 acquisitions were  
230 measured for each sample. The maximum electron transport rate ( $\text{ETR}_{\text{max}}$ ), initial slope of the rapid light curve ( $\alpha$ ), and the  
231 light-saturation parameter ( $E_k$ ) were calculated using the equation described by Platt et al. (1980) without photoinhibition:

232

$$233 \text{ ETR} = \text{ETR}_{\text{max}} \left[1 - e^{-\frac{\alpha E}{\text{ETR}_{\text{max}}}}\right] \quad (5)$$

234

235 These parameters together with the maximum quantum yield of PSII ( $F_v/F_m$ ) were used to compare the photosynthetic  
236 performance of the phytoplankton communities in different microcosms.

237

238 Seawater was sampled before the treatment and at the end of the experiment for particulate trace metal concentrations.  
239 Samples of 100 mL were filtered through an acid-cleaned polycarbonate filter (25 mm diameter, 0.8  $\mu\text{m}$  pore size) and  
240 placed in an acid-cleaned polypropylene filter holder in a trace metal-clean laminar flow bench. The filters were washed  
241 with the EDTA-oxalate reagent (1.4 mL) twice (8 min total) and rinsed with chelexed NaCl solution (0.6 mol L<sup>-1</sup> with 2.38  
242 mmol L<sup>-1</sup> of HCO<sub>3</sub><sup>-</sup>, pH=8.2) 10 times (1.5 mL aliquots) (Tovar-Sanchez et al., 2003; Tang and Morel, 2006). Filters were  
243 stored in acid-washed well plates at -20 °C before analysis. The digestion process followed the method reported by Bowie

244 et al. (2010). Briefly, all samples and triplicate certified reference materials plankton standards (50 mg/vial) were digested  
245 in a mixture of strong ultrapure acids (750  $\mu\text{L}$  12 mol  $\text{L}^{-1}$  HCl, 250  $\mu\text{L}$  40 % HF, 250  $\mu\text{L}$  14 mol  $\text{L}^{-1}$   $\text{HNO}_3$ ) in 15 mL Teflon  
246 perfluoroalkoxy (PFA) vials on a 95 °C hot plate for 12 h in a fume hood. They were then dry evaporated for 4 h and re-  
247 suspended in 10 % v-v ultrapure  $\text{HNO}_3$ . All prepared solutions had indium as internal standard added to a final  
248 concentration of 10  $\mu\text{g L}^{-1}$ . Three pre-mixed multi-element standard solutions (MISA) were prepared as external calibration  
249 standards.

250

251 Particulate organic carbon (POC) was sampled by filtering 100 mL of seawater from each microcosm. Glass fibre filters  
252 (Whatman GF/F, pore size = 0.7  $\mu\text{m}$ , diameter = 13 mm) were pre-combusted at 400 °C for 6 h. Filters were stored at -20 °C  
253 before measurement. Samples were treated via fuming with 2N HCl to remove carbonates overnight and dried in the oven  
254 for 4h. Finally, filters were folded into silver cups and stored in a desiccator until analysis. Samples were analysed for  
255 carbon with a Thermo Finnigan EA 1112 Series Flash Elemental Analyser (CSL, University of Tasmania).

256

257 Biogenic silica (BSi) concentrations were analysed every 4 days by filtering 100 mL of seawater from each microcosm.  
258 Mixed Cellulose Ester (MCE) membrane filters (diameter = 25 mm, pore size = 0.8  $\mu\text{m}$ ) were used for BSi samples. BSi  
259 filters were placed in a plastic petri dish and stored at -20 °C before measurement. Filters were processed using the hot  
260 NaOH digestion method of Nelson et al. (1989). The final solution was measured using the same process as the dissolved  
261 silicate (see section 2.4).

262

263 A self-made plastic zooplankton net (20 mm height and 15 mm width) with a 210  $\mu\text{m}$  mesh size was acid-washed first and  
264 then used to collect zooplankton from microcosms before mineral addition on day 2, near the middle (day 13), and at the  
265 end of the experiment (day 23). Samples were stored in 10 % formalin seawater solutions and kept at room temperature  
266 until measurements. Zooplankton were quantified and identified under a Leica M165C microscope fitted with a Canon 5D  
267 camera. The number of zooplankton from one mini-trawl in each collection was converted to the unit of individual  $\text{L}^{-1}$  and  
268 used for data analysis. The diversity of zooplankton communities was estimated with the Shannon Diversity Index (H)  
269 calculated as:

270

$$271 \quad H = -\sum(pi \times \ln(pi)) \quad (6)$$

272

273 where pi is the proportion of the entire zooplankton community made up of individual species abundance, and ln is the  
274 natural logarithm.

275

276

## 277 **2.6 Statistic analysis**

278 R studio was used for data analyses. Generalized additive models (GAMs) from the package “mgcv” were fitted to the data  
279 to predict the changes over time. The GAMs all shared the same equations:

280

$$281 \quad Y = s(\text{Day}), \quad (7)$$

282



283 in which Y presents the dependent variable and s(Day) is the smooth term of the day of the experiment. Another GAM was  
284 used to detect significant differences between treatments and the control:

$$285 \quad Y = Treatment + s(Day) + s(Day, by = oTreatment) \quad (8)$$

287  
288 In this equation, the variable “Treatment” includes three conditions: “Control”, “Slag” and “Olivine”; while “oTreatment”  
289 is the ordered factor of the variable “Treatment” which allowed us to compare the GAMs smooth terms from different  
290 treatments and the control (Simpson, 2017).

291  
292 When comparing GAMs, P-means represent the p-value obtained from comparing two GAMs, such as the control and the  
293 olivine treatment. If P-means is below 0.05, it indicates that the mean values of the two GAMs exhibit significant  
294 differences over the course of the experiment. Conversely, if P-means is equal to or greater than 0.05, it suggests that the  
295 two GAMs have similar mean values. In contrast, P-smooths represents the p-value derived from comparing the smooth  
296 terms of two GAMs. If P-smooths is below 0.05, it indicates that the two GAMs demonstrate significantly different trends  
297 in their change over time.

298  
299 For the analysis of trace metal concentrations and zooplankton abundance, Generalized Linear Models (GLMs) from the  
300 'stats' package were fitted to the data to determine significant differences between treatments and the control. The selection  
301 of specific GLMs was based on the distribution of the raw data. One GLM equation is

$$302 \quad Y = Treatment + \frac{Day}{22} + \left(\frac{Day}{22}\right)^2 \quad (9)$$

304  
305 with family = Gamma, where Y represents the measured parameter (abundance of a zooplankton species and dissolved  
306 trace metal concentrations); treatment is the conditions (“Control”, “Slag” and “Olivine”); and Day represents the day of  
307 the experiment. The other GLM equation,

$$308 \quad Y = Treatment + Day \quad (10)$$

310  
311 with family = Gaussian, was employed for particulate trace metal data and the Shannon Diversity Index. To compare the  
312 contribution of the three treatments on the measured parameters, Tukey's significant difference test was conducted on the  
313 GLMs using the 'glht' function.

314

### 315 **3. Results**

#### 316 **3.1 Elemental composition and grain size of the finely-ground minerals**

317 SEM analysis revealed the approximate elemental composition of olivine and slag powder (Table 1). Based on this analysis  
318 the olivine composition resembles the Mg-rich olivine mineral “forsterite” (Mg<sub>2</sub>SiO<sub>4</sub>). The particle size spectrum of olivine  
319 powder is shown in detail in Fig. S2. Roughly 69 % of the olivine particles, when measured by volume, fell within the

320 diameter range of 35 - 300  $\mu\text{m}$ . Additionally, SEM analysis revealed high levels of Ca and O in the slag, indicative of the  
 321 considerable  $\text{Ca}(\text{OH})_2$  and  $\text{CaO}$  content of the powder (Table 1; please note that H cannot be measured with the applied  
 322 method). The particle size measurement (Fig. S2) showed that 78 % of the ground slag particles were between 35 - 300  
 323  $\mu\text{m}$ .

324

325 **Table 1.** The weight percentage of elements from two minerals. Unit: wt %.

Element	O	Ca	Mn	Si	Mg	Fe	Al	Ti	Cr	Ni
Olivine	39.9	0.4		19.9	26.4	13.0	1.0			0.8
Steel slag	41.9	36.0	7.0	6.5	4.3	3.7	3.4	1.7	1.6	

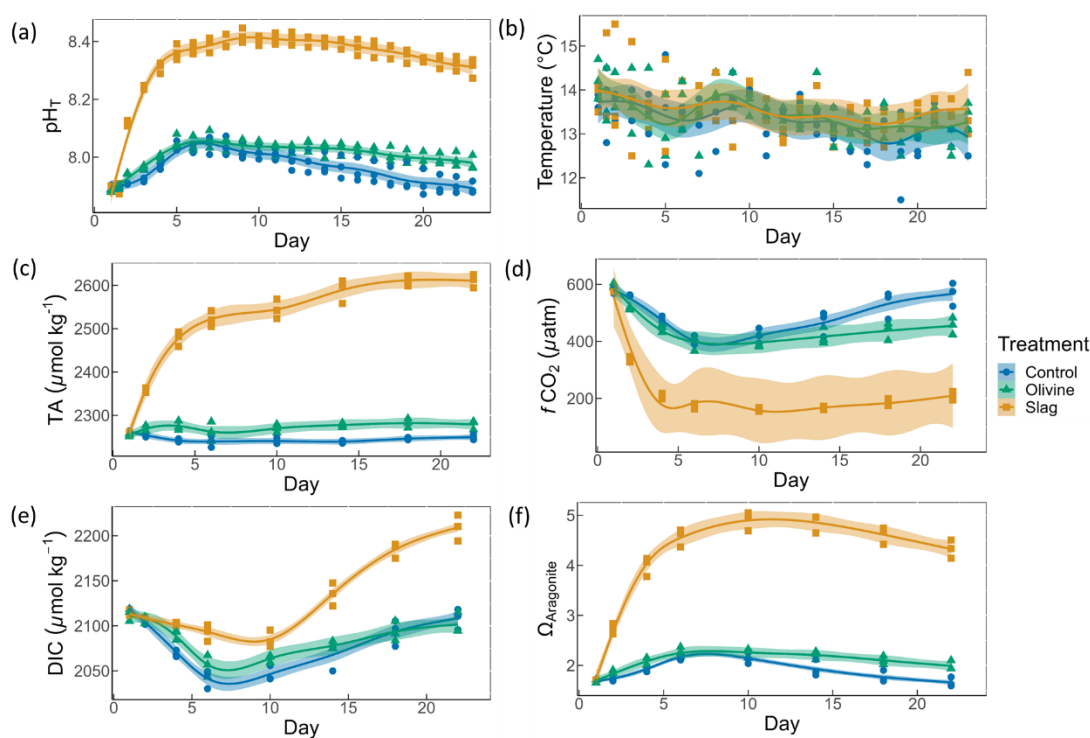
326

327

### 328 3.2 Physical and chemical conditions over the course of the experiment.

329 On day 2 of the experiment, when olivine particles were introduced into the microcosms, the smallest fraction of the powder  
 330 remained suspended, causing the seawater to become highly turbid for several days. The resulting milky appearance of the  
 331 seawater eventually faded over a period of approximately five days, and by day 5, the turbidity had visually become like  
 332 the slag treatment and the control. This effect was not anticipated, and as a result, we decided to investigate its impact on  
 333 light intensity. To do so, a test was conducted after the main experiment in which olivine powder was added to a microcosm  
 334 identical to those used in the experiment, and light intensity was measured daily at a depth of 0.15 m. The results showed  
 335 that the addition of olivine caused an initial reduction in light intensity of 18.5 % at 15 mins after addition, which declined  
 336 to 7.4 %, 3.7 %, 3.7 % and 0 % after 1, 2, 3, and 4 days, respectively. These findings indicate that olivine additions can  
 337 significantly affect the light environment in the microcosms, whereas no such effect was observed in the slag treatment.

338



339

340 **Fig. 2.** Carbonate chemistry conditions. The temporal development of (a)  $\text{pH}_T$ , (b) temperature, (c) total alkalinity (TA), (d)  $\text{CO}_2$  fugacity

341 ( $f\text{CO}_2$ ) computed at *in situ* temperature and atmospheric pressure, (e) dissolved inorganic carbon (DIC), and (f) aragonite saturation state  
 342 ( $\Omega_{\text{aragonite}}$ ). The dots represent the raw data ( $n=3$  for each treatment per sampling time), and the fitted curve is the generalized additive  
 343 model (GAM). The shading represents the 95 % confidence interval of the fitted GAM.

344

345 The  $\text{pH}_T$  of all microcosms increased from day 1 to day 5 (Fig. 2a). This was due to photosynthetic  $\text{CO}_2$  drawdown in the  
 346 control or photosynthetic  $\text{CO}_2$  drawdown in combination with alkalinity release from minerals in the treatments. During  
 347 the peak of the bloom,  $\text{pH}_T$  was  $8.037 \pm 0.010$  in the control (average values  $\pm$  standard error),  $8.054 \pm 0.014$  in the olivine  
 348 treatment and  $8.411 \pm 0.015$  in the slag treatment. The  $\text{pH}_T$  was significantly higher in the slag than the olivine treatment  
 349 and the control throughout the experiment (control and olivine  $\text{pH}_T$  were not significantly different). The  $\text{pH}_T$  on day 23 of  
 350 the control, olivine, and slag treatments were  $7.893 \pm 0.012$ ,  $7.978 \pm 0.015$ , and  $8.309 \pm 0.019$ , respectively. The temperature  
 351 inside of the microcosms varied between replicates, which may have added noise in the biological response data. However,  
 352 on average there was no statistically significant difference between control/treatments during the experiment.

353

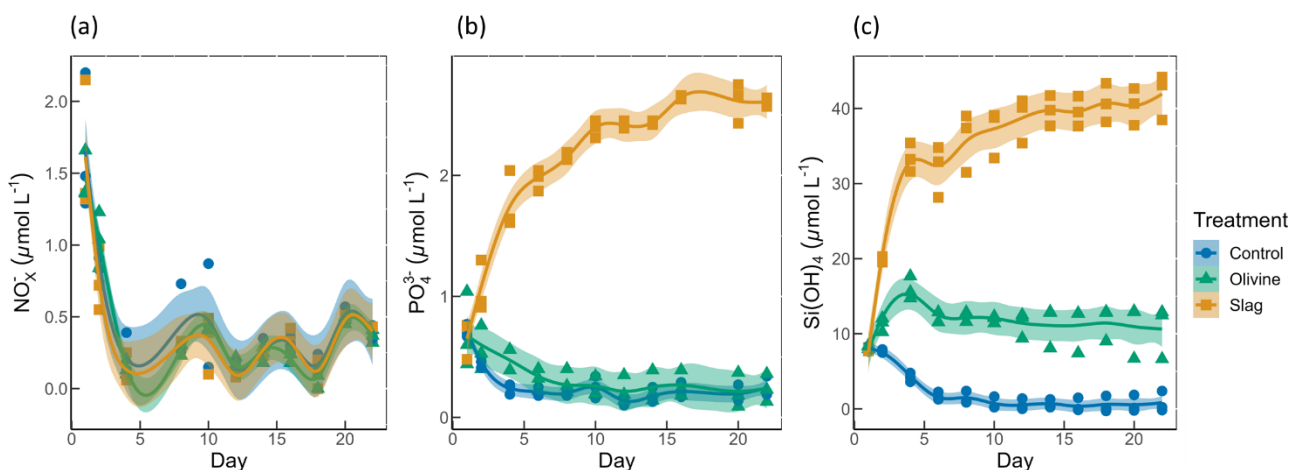
354 In our data analysis, all the fitted GAMs from the treatments and the control exhibited significant differences in  $\text{pH}_T$  from  
 355 each other, as evidenced by the p-values of both P-means and P-smooths being smaller than 0.001. For detailed results of  
 356 the GAM p-values, please refer to Table S2.

357

358 Total alkalinity increased marginally from  $2255 \pm 2$  to  $2262 \pm 13 \mu\text{mol kg}^{-1}$  within the first 6 days after olivine addition  
 359 while it increased more substantially from  $2259 \pm 1$  to  $2522 \pm 11 \mu\text{mol kg}^{-1}$  in the same time span in the slag treatment (Fig.  
 360 2c). The TA in the control decreased from  $2261 \pm 2 \mu\text{mol kg}^{-1}$  to  $2240 \pm 7 \mu\text{mol kg}^{-1}$  from day 1 to day 6 but remained  
 361 stable thereafter. The TA reached  $2279 \pm 6 \mu\text{mol kg}^{-1}$  in the olivine treatment and  $2611 \pm 9 \mu\text{mol kg}^{-1}$  in the slag treatment  
 362 on day 22. The slag treatment reached a significantly higher TA than the olivine treatment and the control (P-smooths <  
 363 0.001). The mean TA from GAM in olivine treatment was higher than the control (P-means < 0.001).

364

365 The  $\text{CO}_2$  fugacity ( $f\text{CO}_2$ ) computed at *in situ* temperature and atmospheric pressure decreased continuously in the first 6  
 366 days in all microcosms (Fig. 2d). Then it increased again in the control and olivine treatments while staying lower in the  
 367 slag treatment (P-means and P-smooths  $\leq 0.001$  between either treatment or the control). Dissolved inorganic carbon (Fig.  
 368 2e) and the aragonite saturation state ( $\Omega_{\text{aragonite}}$ ; Fig. 2f) revealed a similar trend over the course of the experiment in the  
 369 control and the olivine treatment. In contrast, the slag treatment had higher DIC and  $\Omega_{\text{aragonite}}$  values throughout the  
 370 experiment (P-means < 0.001).



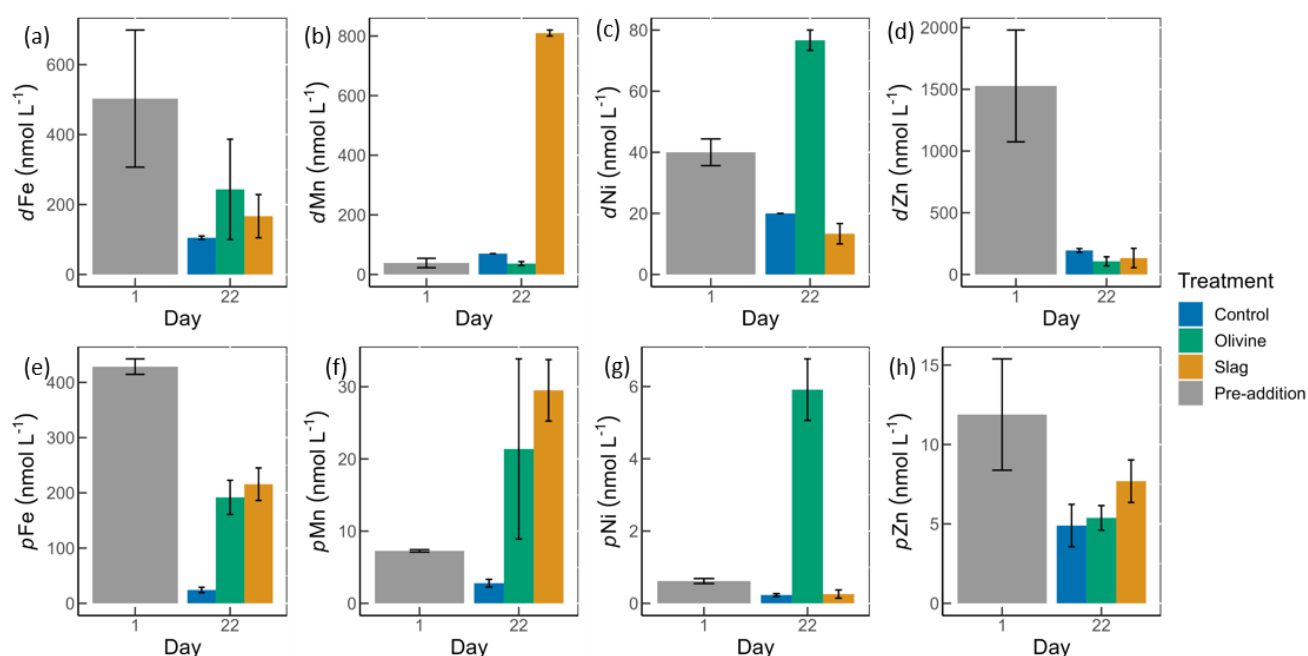
371

372 **Fig. 3.** Macronutrients concentrations over the course of the study. (a) Nitrate and nitrite concentrations. (b) Phosphate concentrations.  
 373 (c) Silicic acid concentrations. The dots represent the raw data ( $n=3$  for each treatment per collection), and the fitted curve is the  
 374 generalized additive model.

375

376 Initial nitrate and nitrite ( $\text{NO}_x^-$ ), phosphate ( $\text{PO}_4^{3-}$ ), and silicic acid ( $\text{Si}(\text{OH})_4$ ) concentrations were  $1.58 \pm 0.12$ ,  $0.69 \pm 0.59$ ,  
 377 and  $8.04 \pm 0.10 \mu\text{mol L}^{-1}$ , respectively (Fig. 3).  $\text{NO}_x^-$  declined rapidly in all microcosms once the experiment had  
 378 commenced to values below  $0.5 \mu\text{mol L}^{-1}$  and no significant difference was detected between treatments and control ( $P$ -  
 379 smooths  $>0.05$ ; Fig. 3a). In both the olivine treatment and the control, the  $\text{PO}_4^{3-}$  concentration decreased in the first six  
 380 days (Fig. 3b). In the slag treatment,  $\text{PO}_4^{3-}$  increased to a maximum of  $2.65 \pm 0.01 \mu\text{mol L}^{-1}$ , which was significantly higher  
 381 than in the olivine treatment and the control ( $P$ -means  $<0.001$ ). The  $\text{Si}(\text{OH})_4$  concentration increased to a maximum of  
 382  $15.99 \pm 0.87 \mu\text{mol L}^{-1}$  in the olivine treatment, increased to a maximum of  $41.92 \pm 1.75 \mu\text{mol L}^{-1}$  in the slag treatment, but  
 383 decreased below the detection limit in the control (Fig. 3c). Significant differences were observed in the development of  
 384  $\text{Si}(\text{OH})_4$  between all treatments and the control (Table S2).

385



386

387

388 **Fig. 4.** Dissolved and particulate trace metal concentrations in microcosm seawater. (a)-(d) are dissolved trace metal concentrations, and  
 389 (e)-(h) are total particulate trace metal concentrations. The error bars represent the standard error from measured samples. The pre-  
 390 addition data shown in (a)-(d) represent the average of 7 microcosms before addition of slag or olivine. The data for the control on day  
 391 22 in (a)-(d) and for the pre-addition on day 1 in (e)-(h) were based on two of three microcosm replicates. The remaining data were based  
 392 on all three microcosm replicates.

393

394 The dissolved trace metal concentrations measured from microcosms are presented in Fig. S3. While the mass of olivine  
 395 added to the microcosms was 50-fold greater than in steel slag (100 g vs 2 g), it's noteworthy that the variation in dissolved  
 396 trace metal concentrations between the two treatments were much smaller than 50 folds. After 21 days of experiment, the  
 397 treatments showed an increase in dissolved Al concentrations from  $920 \pm 286$  to  $970 \pm 228 \text{ nmol L}^{-1}$  in olivine treatment,  
 398 and from  $920 \pm 286$  to  $1093 \pm 77 \text{ nmol L}^{-1}$  in slag treatment, while in the control dissolved Al decreased to  $230 \pm 10 \text{ nmol}$

399 L<sup>-1</sup> (Fig. S3). The fitted GLMs were compared, and the p-value revealed how much influence a treatment had on the  
400 dissolved metal concentrations (Table S3). The results indicate that the slag and olivine additions led to significantly higher  
401 Al concentrations than in the control (p-values < 0.05), but no significant difference was found between the two treatments  
402 (p-value = 0.189). The Cu concentration in the olivine on day 22 was significantly higher than the slag treatment and the  
403 control (p-value < 0.05) (Fig. S3). The addition of olivine and slag released some dissolved Fe, but overall, the concentration  
404 of Fe did not differ significantly between treatments (Fig. 4a, Table S3). The slag released a substantial amount of dissolved  
405 Mn (maximum 810 ± 10 nmol L<sup>-1</sup> on day 22) (Fig. 4b), leading to significantly higher concentrations than in the olivine  
406 treatment and the control (p-values < 0.001). A significant amount of dissolved Ni (maximum 77 ± 3 nmol L<sup>-1</sup> on day 22)  
407 was released from the olivine powder (p-values < 0.001) (Fig. 4c). The initial concentration of dissolved Zn in seawater  
408 was much higher than on day 22 in all microcosms, and no significant difference in Zn concentrations was found between  
409 the treatments and the control.

410

411 Particulate concentrations of some trace metals also differed between treatments. The total particulate Fe decreased in all  
412 microcosms on day 22 comparing with the pre-addition level, but both mineral addition treatments had higher particulate  
413 Fe concentrations than the control (Fig. 4e). The addition of slag elevated particulate Mn concentrations to a level higher  
414 than the pre-addition and the control on day 22 (Fig. 4f), while the addition of olivine increased the particulate Ni  
415 concentrations to a level higher than the slag, the control, and the pre-addition (Fig. 4g). The particulate Zn concentrations  
416 in general decreased by the end of the experiment (Fig. 4h), and no significant differences were found between the  
417 treatments and the control.

418

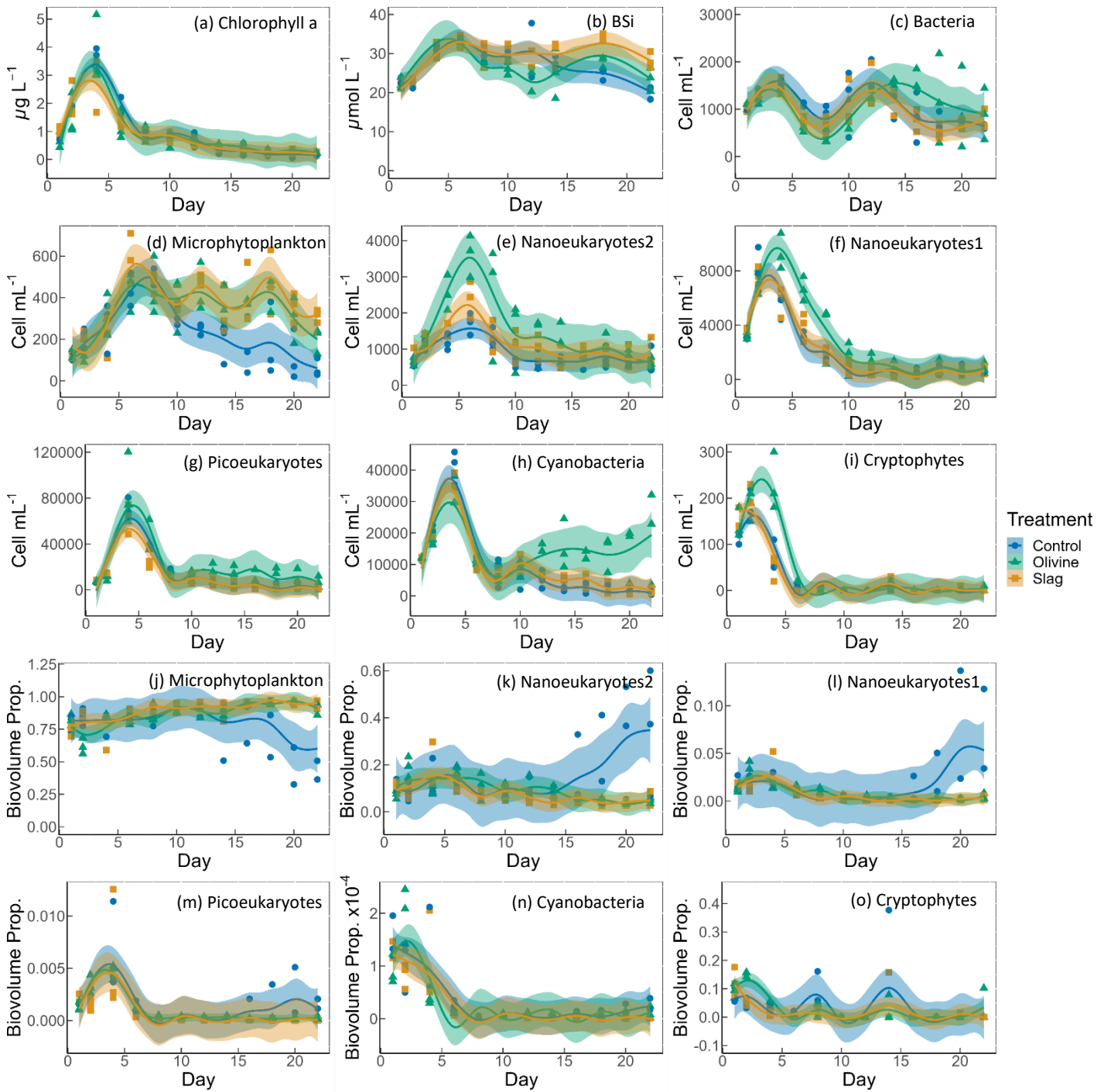
419 The POC on day 1 and day 22 from all microcosms were very similar, 10.99 ± 0.58 and 11.03 ± 0.41 μmol L<sup>-1</sup> respectively  
420 (Fig. S4) so the metal:POC results were consistent with the particulate trace metal results (Fig. 4 e-h). In general, the non-  
421 surface metal:POC are positively correlated with the total metal:POC ratios (Fig. S5). The ratio of non-surface to total  
422 particulate trace metal concentrations is summarized in Table S5. Both non-surface and total Fe concentrations decreased  
423 in microcosms on day 22 compared with the pre-addition level. Iron:POC ratios were significantly higher in the treatments  
424 than in the control on day 22 (p-values < 0.05, Table S3), and there was no significant difference between mineral addition  
425 treatments. The non-surface to total Fe:POC ratios were > 0.94 in all microcosms on both day 1 and day 22. The total and  
426 non-surface Mn:POC ratio was the highest in the slag treatment. These ratios were higher than the pre-addition level and  
427 the control at the end of the experiment. The total particulate Ni concentrations in the olivine treatment were significantly  
428 higher than before olivine addition. The olivine treatment led to a >22-fold higher Ni:POC ratio compared to the other two  
429 treatments (p-value < 0.001).

430

431

432

433 **3.3 Development and physiology of the plankton community**



434  
 435 **Fig. 5.** Temporal development of chlorophyll a concentration (chl-a), BSi, and different eukaryotic and bacterial plankton groups as  
 436 determined with flow cytometry. (a) chlorophyll a; (b) BSi; cell concentrations of (c) heterotrophic bacteria, (d) microphytoplankton, (e)  
 437 nanoeukaryotes2, (f) nanoeukaryotes1 (g) picoeukaryotes, (h) cyanobacteria, and (i) cryptophytes; biovolume proportion of (j)  
 438 microphytoplankton, (k) nanoeukaryotes2, (l) nanoeukaryotes1 (m) picoeukaryotes, (n) cyanobacteria, and (o) cryptophytes. The figure  
 439 data points represent the raw data, and the fitted curve is the generalized additive model. The shaded area represents the 95 % confidence  
 440 interval.

441

442 The chl-a concentration in all microcosms increased from day 1 to day 4 from  $1 \mu\text{g L}^{-1}$  to  $3\text{-}4 \mu\text{g L}^{-1}$  (Fig. 5a). The chl-a  
443 concentration then decreased rapidly from day 4 to day 8, then continued to decrease, though more slowly, to  $<0.3 \mu\text{g L}^{-1}$   
444 until the end of the experiment. The GAMs of chl-a did not show any difference between treatments and the control (both  
445 P-means and P-smooths  $>0.05$ , see Table S2).

446

447 The BSi concentration increased from day 1 to day 6 in all microcosms (Fig. 5b). In the olivine treatments, BSi  
448 concentrations decreased slightly after the peak until day 12 but then increased again. In the slag treatment, BSi  
449 concentrations remained relatively stable after the initial phytoplankton bloom. In contrast, BSi concentration decreased  
450 continuously in the control after the initial peak. Olivine particles suspended in seawater after the mineral addition (see  
451 section 3.2) partially ended up on BSi filters during filtration. This led to extremely high BSi measurements on days 2 and  
452 4 that were removed from Fig. 5b. Without these outliers, the mean of fitted BSi GAM in the olivine treatment was lower  
453 than the control and the slag treatment (Table S2), and the slag treatment had the highest average BSi over the course of  
454 the experiment. Overall, the BSi trends in the two treatments were similar (P-smooths = 0.269), and both were significantly  
455 different from the control (P-smooths  $<0.05$ ).

456

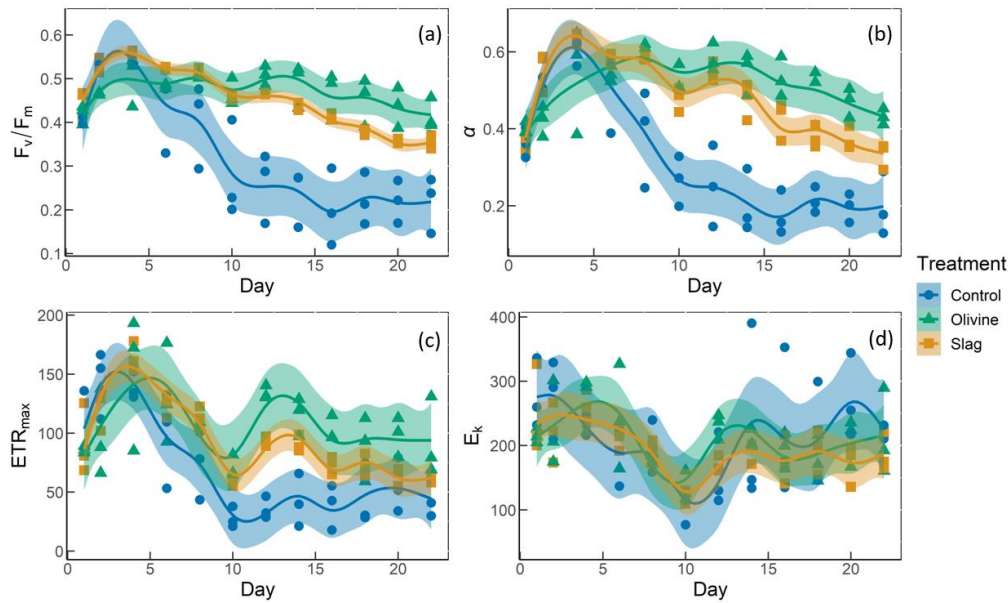
457 The development of the phytoplankton community composition showed significant differences between the treatments and  
458 the control. In general, most phytoplankton groups exhibited similar patterns to chl-a, with peak cell numbers occurring on  
459 day 4 (Fig. 5f-i) apart from microphytoplankton and nanoeukaryotes2 which had the peak delayed for 1-2 days (Fig. 5d-  
460 e). Please be aware that flow cytometers may not capture some large and chain-forming phytoplankton. After reaching  
461 peak values during the bloom, phytoplankton abundance generally decreased steadily. Microphytoplankton displayed  
462 similar trends to the results for BSi. Before day 10, all microcosms had similar microphytoplankton abundances (Fig. 5d).  
463 However, in the control, microphytoplankton abundance declined continuously and at a faster rate compared to the two  
464 treatments (P-smooths values  $<0.03$ ). From day 2 to day 6, the abundance of nanoeukaryotes1, nanoeukaryotes2,  
465 picoeukaryotes, and cryophytes was higher in the olivine treatment compared to the slag treatment and the control. After  
466 day 8, their abundance in the olivine treatment decreased to a similar level as the slag treatment and the control. Notably,  
467 there were few significant differences observed between the slag treatment and the control in terms of the abundances of  
468 nanoeukaryotes1, nanoeukaryotes2, picoeukaryotes, cyanobacteria, and cryptophytes throughout the experiment. In the  
469 olivine treatment, cyanobacteria experienced a second bloom after day 10, which was significantly different from the other  
470 two groups (P-smooths  $<0.01$ ). Heterotrophic bacteria exhibited an increase and decline pattern following the  
471 phytoplankton bloom until day 8 (Fig. 5c). Subsequently, bacteria abundance increased again, reaching a second peak  
472 during days 12-14, followed by a decline until the end of the experiment. The decline in bacteria abundance was slower in  
473 the olivine treatment, although no significant differences were detected between treatments (Table S2).

474

475 Among all the microcosms, microphytoplankton consistently accounted for the largest proportion of biovolume. From the  
476 perspective of biovolume proportion, the mineral addition mainly influenced the microphytoplankton and nanoeukaryotes.  
477 The control had similar phytoplankton biovolume distribution as the treatments from day 1 to day 15, but after that the  
478 proportion of microphytoplankton biovolume decreased to a level significantly lower than the treatments. In the control  
479 treatment, the proportion of nanoeukaryotes' biovolume increased as the proportion of microphytoplankton decreased. The  
480 biovolume of picoeukaryotes, cyanobacteria and cryptophytes increased during the phytoplankton bloom and then  
481 decreased drastically after the bloom. There were no significant differences in biovolume proportion observed for

482 picoeukaryotes, cyanobacteria and cryptophytes between the treatments and the control.

483



484

485 **Fig. 6.** The photosynthetic performance of the phytoplankton community. (a)  $F_v/F_m$ , the maximum quantum yield of photosynthesis II.  
486 (b)  $\alpha$ , the initial slope of the rapid light curves. (c)  $ETR_{max}$  is the maximum electron transport rate, the maximum potential photosynthetic  
487 rate. (d)  $E_k$  is light-saturation parameter, Unit:  $\mu\text{mol photons m}^{-2} \text{s}^{-1}$ .

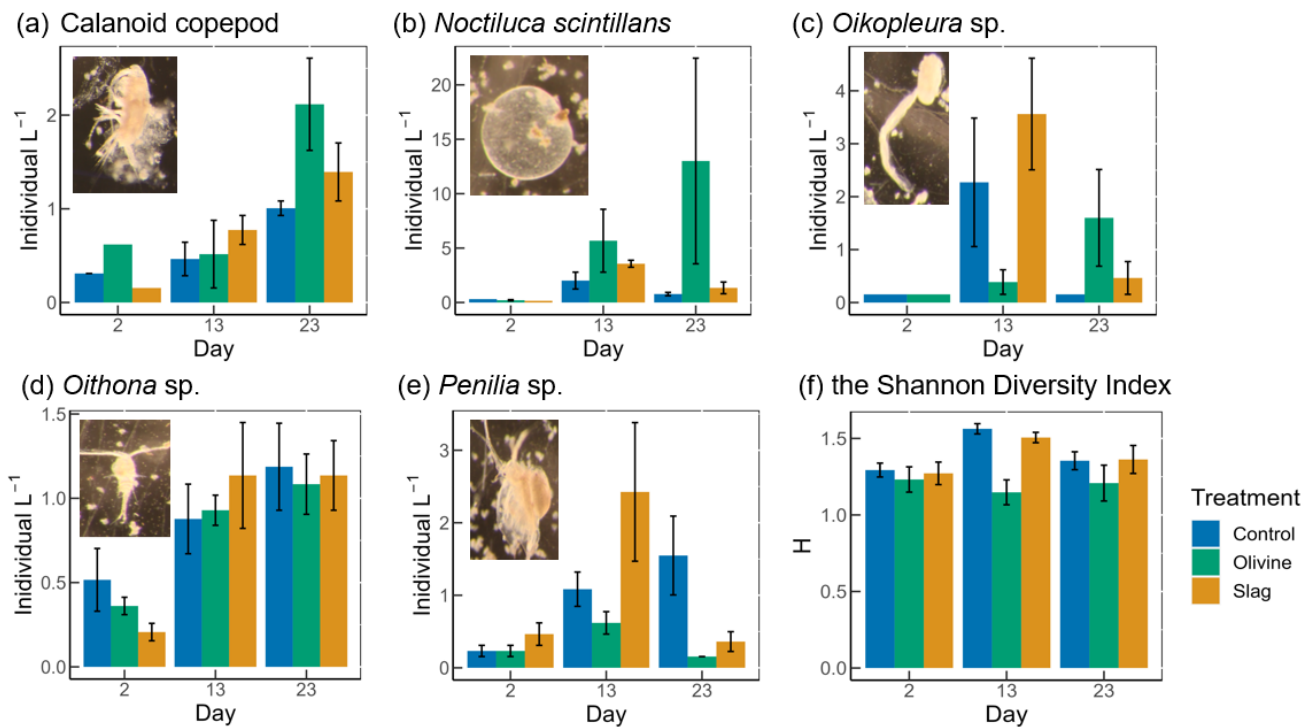
488

489 The temporal development of  $F_v/F_m$ ,  $\alpha$ ,  $ETR_{max}$ , and  $E_k$  is illustrated in Fig. 6. The  $F_v/F_m$  values of the phytoplankton  
490 community were approximately  $0.42 \pm 0.01$  and increased to levels  $> 0.5$  during the peak of the phytoplankton bloom on  
491 day 4 (Fig. 6a). Following the bloom,  $F_v/F_m$  values dropped below 0.3 in the control. However, the decline in  $F_v/F_m$  after  
492 the bloom was less pronounced in the two mineral addition treatments with the olivine treatment maintaining higher  $F_v/F_m$   
493 values than the slag treatment (P-smooths  $< 0.05$ ). At the end of the experiment,  $F_v/F_m$  was  $0.22 \pm 0.04$  in the control,  $0.35$   
494  $\pm 0.01$  in the slag treatment, and  $0.42 \pm 0.02$  in the olivine treatment. The temporal development of  $\alpha$  aligned with the  
495 patterns observed for  $F_v/F_m$  (compare Fig. 6a and 6b). The maximum values of  $ETR_{max}$  were observed on day 4 in the  
496 control and the slag treatment, while in the olivine treatment, it occurred on day 5 (Fig. 6c). Subsequently,  $ETR_{max}$   
497 continuously decreased until day 10 and then stabilized until the end of the experiment. However,  $ETR_{max}$  exhibited a  
498 subsequent increase in the mineral treatments around day 12. The  $ETR_{max}$  values were higher in the mineral treatments  
499 compared to the control group (P-means  $< 0.001$ , Table S2). The parameter  $E_k$  decreased from  $246 \pm 17 \mu\text{mol photons m}^{-2}$   
500  $\text{s}^{-1}$  on day 1 to  $121 \pm 7 \mu\text{mol photons m}^{-2} \text{s}^{-1}$  on day 10, and then it increased again to approximately  $200 \mu\text{mol photons m}^{-2}$   
501  $\text{s}^{-1}$  by the end of the experiment (Fig. 6d). The change in  $E_k$  did not exhibit significant differences between the treatments  
502 and the control (both P-means and P-smooths  $> 0.05$ ).

503

504





505

506 **Fig. 7.** The dominant zooplankton abundance and community diversity from different treatments. Abundance of dominant zooplankton  
 507 in microcosms: (a) calanoid copepod; (b) *Noctiluca scintillans*; (c) *Oikopleura* sp.; (d) *Oithona* sp.; (e) *Penilia* sp.; and (f) the Shannon  
 508 diversity index (H) of different treatments and the control. Error bars represent the standard error calculated from three microcosm  
 509 replicates. Photographs of each zooplankton group are shown on the corresponding graphs.

510

511 Thirteen zooplankton taxonomic groups were identified in the microcosms. The dominant taxa were the appendicularian  
 512 *Oikopleura* sp., the cyclopoid copepod *Oithona* sp., the cladoceran *Penilia* sp., the heterotrophic dinoflagellate *Noctiluca*  
 513 *scintillans* and several calanoid copepods including *Acartia* sp., *Paracalanus* sp. and *Gladioferens* sp. The larvae and eggs  
 514 of *Oikopleura*, *Penilia* and copepod were also observed under the microscope. In general, higher zooplankton numbers  
 515 were observed after the bloom on day 13 (Fig. 7). The abundance of calanoid copepods and *Oithona* sp. increased after  
 516 day 2 (Fig. 7a, d), and there was no significant difference between treatments and the control (p-values >0.05, Table S4).  
 517 The abundance of *N. scintillans* increased significantly more in the olivine treatment than in the control and the slag  
 518 treatment, with highest abundance of  $13 \pm 9$  individual L<sup>-1</sup> observed in the olivine treatment on the last day (Fig. 7b). The  
 519 abundance of *Oikopleura* in the control and the slag treatment was higher than the olivine treatment on day 13 but was  
 520 higher in the olivine treatment on day 22 (Fig. 7c). A higher abundance of *Penilia* sp. was found in the slag treatment on  
 521 day 13 and in the control on day 23 (Fig. 7e). Due to the patchy distribution of zooplankton, these data have large standard  
 522 errors and only the differences in the numbers of *N. scintillans* in the olivine treatment were statistically significantly  
 523 different from the slag treatment and the control (p-value <0.05, Table S4).

524

525 Considering the control and slag treatment, the Shannon Diversity Index (H) increased from day 2 to day 13 and declined  
 526 on day 23, while in the olivine treatment, H was lower on day 13 than on day 2 and day 23 (Fig. 7f). The GLMs revealed  
 527 that the olivine treatment had significantly lower H on day 13 than the control and the slag treatment (p-values <0.001).  
 528 There were no significant differences in H between the control and the slag treatment (Table S4). The addition of olivine  
 529 decreased the zooplankton community's diversity. This is mainly driven by distinct trends observed in the abundance of  
 530 *Oikopleura* sp., *Penilia* sp., and *N. scintillans* (Fig. 7).

531

## 532 **4. Discussion**

### 533 **4.1 CO<sub>2</sub> removal potential of slag and olivine**

534 The slag powder created significantly higher CO<sub>2</sub> removal potential than the olivine powder over the course of the study.  
535 Ca(OH)<sub>2</sub> and CaO in slag and Mg<sub>2</sub>SiO<sub>4</sub> in olivine are likely to be the main functional minerals driving the measured  
536 alkalinity enhancement. Total alkalinity increased by 361 μmol kg<sup>-1</sup> in the slag treatment while it increased by only 29  
537 μmol kg<sup>-1</sup> in the olivine treatment, equivalent to a potential increase in marine inorganic carbon by 14.7 and 0.9% within  
538 3 weeks of their application. When normalizing these alkalinity increases to the same material weight, 1 g of slag would  
539 release 9626 μmol TA while 1 g of olivine would release 16 μmol TA. Thus, over 3 weeks of experimental incubation, slag  
540 is ~600-fold more efficient in releasing alkalinity for particles of this size class (please note that particle size spectra of  
541 olivine and slag were similar but not identical; Fig. S1). We can also use these values to make a rough estimate of how  
542 much CO<sub>2</sub> these two minerals could potentially sequester. One mole of alkalinity from olivine and slag can sequester  
543 approximately 0.85 mole of CO<sub>2</sub>. Thus, one tonne of slag and olivine powder as used here could sequester 360 and 0.6 kg,  
544 respectively, within 3 weeks. It is likely that optimization of particle size and application method may lead to higher  
545 efficiencies. Nevertheless, the slag showed potential as an OAE source mineral, even when applied as relatively coarse  
546 powder in this experiment.

547

### 548 **4.2 Environmental implications of slag and olivine additions**

549 The amount of olivine and slag powder added to the treatments differed significantly (100 g of olivine powder were added  
550 while only 2 g of slag powder were added to the 53 L microcosms). Our rationale for these different mass additions was to  
551 yield somewhat similar amounts of detectable alkalinity enhancement in the dissolved phase, since we already knew from  
552 tests before the experiment that slag elevates alkalinity faster than olivine. However, olivine was less efficient in releasing  
553 alkalinity than we had anticipated so that even a 50-fold higher addition of olivine (in mass) did not compensate for this  
554 difference. As such, our experiments are associated with an “apples and oranges issue” in that our perturbation with  
555 minerals and associated OAE differs. To account for this, the following discussion mainly relates the observed  
556 environmental effects with the alkalinity enhancement achieved over the course of the study.

#### 557 **4.2.1. OAE effects on phytoplankton physiology and community**

558 Previous research has hypothesised that OAE-induced changes in seawater carbonate chemistry could delay phytoplankton  
559 bloom formation due to reductions in seawater *p*CO<sub>2</sub> in the aftermath of an OAE deployment (Bach et al., 2019). The build-  
560 up of chlorophyll *a* concentration as observed here was indistinguishable between treatments and the control, suggesting  
561 no effect of slag- or olivine-based OAE on phytoplankton bloom dynamics under these experimental settings. A lack of  
562 bloom delay due to carbonate chemistry is unsurprising for the olivine treatment where the release of alkalinity was small  
563 (29 μmol kg<sup>-1</sup> alkalinity release), but somewhat more surprising in the slag treatment where alkalinity was quite rapidly  
564 increased by 361 μmol kg<sup>-1</sup>. However, the release was still lower than in a very similar study by Ferderer et al., (2022)  
565 where alkalinity was increased by 500 μmol kg<sup>-1</sup> using sodium hydroxide and even there they did not observe a bloom

566 delay. Based on this very limited evidence, it seems that bloom delays do not occur consistently under OAE within the  
567 alkalinity ranges tested in this study.

568

569 The nutrient data show that the phytoplankton community was most likely N-limited after day 4 so that the release of  
570  $\text{Si(OH)}_4$  from olivine and  $\text{Si(OH)}_4$  and  $\text{PO}_4^{3-}$  from slag did not stimulate a further increase in chlorophyll-*a* concentration  
571 in the treatments. The development of BSi concentrations is indicative of the prevalence of diatoms in the microcosms but  
572 differences between treatments and the control were small. The release of  $\text{Si(OH)}_4$  through olivine and slag will most likely  
573 benefit diatoms but this fertilization effect did not manifest in this specific experiment because N was limiting diatom  
574 growth. However, when new N is supplied then diatoms will likely take a bigger share of the limiting N pool when olivine  
575 or slag are used for OAE, as has been shown in  $\text{Si(OH)}_4$  manipulation experiments in and outside the context of OAE  
576 research (Egge and Jacobsen, 1997; Ferderer et al., 2023). In the case of slag, the release of  $\text{PO}_4^{3-}$  will likely be another  
577 driver that affects plankton productivity and community composition. As for  $\text{Si(OH)}_4$ , however, the effect of additional  
578  $\text{PO}_4^{3-}$  did likely not materialise in this experiment because  $\text{PO}_4^{3-}$  was not limiting over the course of the study. However, in  
579 ecosystems where  $\text{PO}_4^{3-}$  is a limiting resource, the application of slag could enhance productivity with associated benefits  
580 for higher trophic levels. In contrast, excessive applications of slag and concomitant  $\text{PO}_4^{3-}$  release could also pose a risk of  
581 eutrophication. Future studies may need to investigate what the most sustainable dose of OAE via olivine and/or slag  
582 applications could be and the suitable regions for application.

583

584 The flow cytometry results further revealed the change in phytoplankton community composition. Both the olivine and  
585 slag treatments sustained higher microphytoplankton abundances after the peak of the phytoplankton bloom. This trend is  
586 consistent with higher  $F_v/F_m$  values in the treatments than in the control so that it is tempting to assume that  
587 photophysiological fitness gain measured with the FRRf led to higher competitiveness of microphytoplankton in the  
588 community. Indeed, calculations of the contribution of different phytoplankton groups to total biovolume based on flow  
589 cytometry indicate that microphytoplankton were predominantly contributing to the phytoplankton community biovolume  
590 so that the responses measured by the FRRf were probably to a large extent driven by this group.

591

592 Apart from the increased microphytoplankton abundance, for the slag treatment, other phytoplankton groups distinguished  
593 with flow cytometry did not deviate considerably from the control. The olivine addition, however, triggered more  
594 pronounced shifts in the phytoplankton community. In particular, the nanoeukaryotes (roughly between 2-20  $\mu\text{m}$ ),  
595 picoeukaryotes and the cryptophytes showed relatively higher abundance during the peak of the phytoplankton bloom, and  
596 the abundance of cyanobacteria was higher after the bloom. We speculate that this shift following olivine treatment may  
597 be attributable to a top-down effect from the decrease in zooplankton grazing effects in microcosms, which will be  
598 discussed in section 4.2.2.

599

600 The measurement of photophysiological parameters revealed that the phytoplankton had generally better photosynthetic  
601 performance in the slag and olivine treatments than in the control, especially after the phytoplankton bloom. During the  
602 first 5 days, the changes in phytoplankton photosynthetic performance were indistinguishable between the control and the  
603 slag treatment, while the values of  $\alpha$ ,  $\text{ETR}_{\text{max}}$  and  $F_v/F_m$  were lower in olivine treatment. At this time all microcosms had  
604 similar health because of the relatively high  $\text{NO}_x^-$  concentrations and Fe supply (around 500  $\text{nmol L}^{-1}$ ), but the suspended  
605 particles in the olivine treatment may have led to artifacts in the measuring of photophysiology by FRRf. Scattering and/or

606 absorption of light by suspended olivine particles is the most parsimonious explanation for the simultaneous depression in  
607  $\alpha$ ,  $ETR_{max}$  and  $F_v/F_m$ . After day 5, the  $F_v/F_m$ ,  $\alpha$  and  $ETR_{max}$  values decreased significantly faster in the control than in the  
608 treatments, and to values lower than the initial condition. A decrease of  $F_v/F_m$  is commonly associated with physiological  
609 stress, such as nutrient limitation, and high light stress (Bhagooli, et al., 2021), with Fe limitation causing a more  
610 pronounced decline in  $F_v/F_m$  than nitrogen limitation (Gorbunov, et al., 2021). The  $ETR_{max}$ , which represents the maximum  
611 electron transport rate, has also been shown to be negatively affected when phytoplankton experience nitrogen or Fe  
612 limitation (Kolber et al., 1994; Gorbunov & Falkowski 2021). Furthermore, the change in photosynthesis performance  
613 after day 10 was suspected to be driven by the microphytoplankton because the decrease of  $F_v/F_m$ ,  $\alpha$ , and  $ETR_{max}$  in the  
614 control was coupled with the decrease in microphytoplankton abundance while the other phytoplankton groups were in  
615 low abundance as in the mineral addition treatments, and the microphytoplankton contributed significantly (75 %) to  
616 community biovolume. All microcosms were similarly  $NO_x^-$  limited from day 5 onward (Fig. 3) so that N-limitation is  
617 unlikely to explain different trends in photophysiological parameters between the control and OAE treatments. Trace metals,  
618 especially Fe, released through slag and olivine additions could potentially explain these differences.

619  
620 Several of the trace metals released from slag and olivine are required for photosynthesis. For example, Fe is required for  
621 many proteins functioning in photosynthesis, such as cytochromes, ferredoxin, and superoxide dismutase (SOD) (Twining  
622 and Baines, 2013), and the addition of Fe can stimulate the growth of phytoplankton (Sunda and Huntsman, 1997) and  
623 increase  $F_v/F_m$  (Behrenfeld et al., 2006). The dissolved and particulate Fe concentrations were higher in mineral addition  
624 treatments than in the control indicating potentially more Fe available to sustain phytoplankton photosynthesis. While this  
625 explanation is intriguing for the observed trends in photophysiology, it remains unclear why such strong differences  
626 occurred between mineral addition and control treatments despite dissolved Fe concentrations of  $\sim 500 \text{ nmol L}^{-1}$  at the end  
627 of the experiment in the control. In Fe-limited ocean regions, dissolved Fe is at least two orders of magnitude lower, and  
628 the enhancement of Fe to  $\sim 1.5 \text{ nmol L}^{-1}$  can induce major phytoplankton blooms and relieve photophysiological stress (De  
629 Baar et al., 2005). It is possible that these coastal phytoplankton species have higher Fe requirements than those from the  
630 open ocean where Fe is limiting (Strzepek and Harrison, 2004). Our findings suggest that Fe perturbations may not only  
631 be relevant for low Fe open ocean regions but could also be relevant for coastal ocean locations.

632  
633 Alternatively, the addition of Mn, Ni and other trace metals from mineral addition may have benefited photosynthesis.  
634 Manganese is required for the water-splitting reaction of photosystem II (Armstrong, 2008), and both Mn and Ni are  
635 common bioactive trace metals for SODs in marine phytoplankton. The noxious superoxide anion radical ( $O_2^-$ ) generated  
636 from aerobic respiration and oxygenic photosynthesis could be harmful to phytoplankton physiology, and SOD removes  
637  $O_2^-$ , thus improving photosynthesis (Wafar et al., 1995; Wolfe-Simon et al., 2005). This is consistent with our  
638 photosynthetic measurements. Interestingly, although the amounts and types of trace metals released from the slag and  
639 olivine powders were different, they led to relatively similar  $F_v/F_m$  values with only slightly higher  $F_v/F_m$  in the olivine  
640 than the slag treatment from days 10-21. Over this time, these trace metal additions could have fertilized different  
641 phytoplankton species (Pausch et al., 2019; Balaguer et al., 2022; Guo et al., 2022) possibly because different  
642 phytoplankton could have different trace metal requirements, such as for SOD. For example, cyanobacteria have NiSOD,  
643 diatoms have MnSOD, dinoflagellates have both FeSOD and MnSOD (Wolfe-Simon et al., 2005). Another explanation is  
644 that phytoplankton in the control were limited by bicarbonate while the treatments had sufficient bicarbonate from added  
645 minerals. However, we were unable to determine the species-level changes in the phytoplankton community, and hence

646 whether these trace metals, individually or combined, could account for the observed phytoplankton community  
647 photosynthetic performance.

648

#### 649 4.2.2. OAE impacts on the zooplankton community

650 Slag-based OAE did not significantly influence the zooplankton community composition while olivine-based OAE induced  
651 some statistically significant effects, including a lower Shannon diversity. The increase in *N. scintillans* abundance and the  
652 decrease in *Penilia* sp. and *Oikopleura* sp. in the olivine treatment indicate that the zooplankton response to OAE can vary  
653 among different zooplankton types.

654

655 The observed lower abundance of *Oikopleura* sp. on day 13 in the olivine treatment may indicate a temporary suppression  
656 or a slower growth rate of this zooplankton species in response to the olivine addition. This could be attributed to the  
657 potential effects of olivine on the availability of essential nutrients or changes in the physicochemical environment of the  
658 water. However, the subsequent increase in *Oikopleura* sp. abundance by day 22 suggests that the growth of this species  
659 may have recovered or accelerated in the olivine treatment, leading to a higher abundance compared to the slag treatment  
660 and the control on day 22. As discussed in section 4.2.1, reduced *Oikopleura* sp. abundance was unlikely due to reduced  
661 food availability since phytoplankton within the preferred edible size spectrum, such as cyanobacteria and nanoeukaryotes,  
662 were even more abundant in the olivine treatment. Instead, we hypothesize it to be an effect of the suspended olivine  
663 particles that occurred for approximately the first 5 days of the study that were so plentiful that they turned the enclosed  
664 seawater milky and may have clogged the mucous feeding mesh of *Oikopleura* sp. (Lombard et al., 2011).

665

666 The abundance of *Penilia* sp. and *Oikopleura* sp. was lower in the olivine treatment than the other two groups throughout  
667 the experiment while the abundance of *N. scintillans* was consistently higher. The second bloom of cyanobacteria in olivine  
668 is potentially the results of decreased predators, like *Penilia* sp. and *Oikopleura* sp.. We cannot provide a particularly  
669 convincing hypothesis about what specifically drove these in these zooplankton species, although it is tempting to speculate  
670 that suspended particles present in the olivine treatment at the beginning may have played a role also for those organisms  
671 since this was the only apparent systematic difference to the control and slag treatment. The proliferation of *N. scintillans*  
672 can be problematic since heterotrophic dinoflagellate blooms can regulate phytoplankton communities, cause toxicity to  
673 aquatic fish, and create a hypoxic sub-surface zone (Baliarsingh et al., 2016; Zhang et al., 2020; Al-Azri et al., 2007),  
674 although a bloom of *N. scintillans* in southeast Australia only induced ichthyotoxicity when the cell concentration reached  
675 2,000,000 cells L<sup>-1</sup> (Hallegraeff et al., 2019). For comparison, we observed a maximum of 32 cells L<sup>-1</sup> in one microcosm  
676 replicate of the olivine treatment.

677

678 In comparison to olivine, steel slag seemed to have less potential to affect zooplankton community composition. The  
679 abundance of all groups of phytoplankton, apart from microphytoplankton after day 10, was similar in the slag treatment  
680 and the control through the experiment. This is probably because the amount of slag powder added in the treatment was  
681 much less than the olivine powder resulting in fewer physical particle perturbations to zooplankton. In addition, the  
682 chemistry perturbations such as enhanced alkalinity concentration and various dissolved trace metals, especially Mn, from  
683 the slag powder did not seem to have a notable direct influence on zooplankton abundance over the three-week period.  
684 Even though we did not observe drastic changes in zooplankton abundance during the experiment, considering there was

685 higher microphytoplankton abundance in the slag treatment after day 10, slag powder may benefit some zooplankton  
686 especially those who feed on large phytoplankton on a longer time scale.

687

#### 688 **4.2.3. Dissolved trace metal accumulation in seawater and its environmental implications**

689 The addition of olivine and slag as OAE source minerals released trace metals into the seawater, predominantly Al, Fe, Ni,  
690 and Cu (olivine) as well as Al, Fe, and Mn (slag). The maximum measured concentrations for dissolved Al, Fe, Ni, Cu, and  
691 Mn were 1093, 253, 77, 27, and 810 nmol L<sup>-1</sup>, respectively. The threshold values for drinking water with health or aesthetic  
692 considerations by the Australian Drinking Water Guidelines for Al, Fe, Ni, Cu, and Mn are 7400, 5360, 340, 15600, and  
693 1800 nmol L<sup>-1</sup>, respectively (NRMMC, 2022). All dissolved trace metal concentrations measured herein are well below  
694 these health and aesthetic threshold values. In natural freshwater sources, the concentrations of Al, Fe, Ni, Cu and Mn are  
695 generally less than 44000, 71400, 510, 156, and 25400 nmol L<sup>-1</sup> (NRMMC, 2022). Although these natural water data were  
696 primarily derived from rivers and streams, they serve as valuable references for evaluating trace metal release in our  
697 experiment. Thus, mineral additions to the microcosms as simulated here did not increase thresholds for any of the  
698 measured trace metals beyond those that are considered safe for drinking water quality, and they were within the trace  
699 metal concentration range in natural water. However, while these guidelines on drinking water provide a good starting point  
700 on how to quantify what OAE perturbation could be considered “safe” and “unsafe” with regards to trace metals, it must  
701 be recognized that seawater is not drinking water and that critical thresholds may be different in the latter.

702

703 The release of trace metals from OAE materials is considered to have relatively strong effects on biology, particularly in  
704 the open ocean where trace metals usually occur in lower concentrations. For example, oceanic Al, Fe, Ni, and Mn  
705 concentrations are about 2, 0.5, 8, and 0.3 nmol L<sup>-1</sup> (Bruland and Lohan, 2003; Sohrin and Bruland, 2011). Previous  
706 research on OAE-associated trace metal impacts on individual phytoplankton species grown in laboratory environments  
707 has shown that concentration thresholds beyond which trace metal induces negative effects on fitness likely differ between  
708 species (Guo et al., 2022; Hutchins et al., 2023; Xin et al., 2023). Indeed, our experiment with plankton communities  
709 provides further support that several components of the planktonic food web are affected by OAE. However, our experiment  
710 does not allow determining whether observed effects were primarily invoked by carbonate chemistry, macronutrient (P and  
711 Si), or trace metal perturbations. Thus, dedicated experiments isolating the impact of these factors on plankton will be  
712 required in the future.

#### 713 **4.2.4. Particulate trace metal accumulation in seawater and its environmental implications**

714 The Derwent Estuary (where we collected our plankton communities) was highly metal polluted due to industrial practice  
715 (Macleod and Coughanowr, 2019). Both our dissolved and particulate trace metal data indicated high background metal  
716 concentrations, especially for Fe and Zn. Furthermore, the metal:POC ratios found here are higher than reported for open  
717 ocean studies or lab cultures. For example, the Fe:POC can vary from 2-136  $\mu\text{mol mol}^{-1}$  depending on the cultured  
718 phytoplankton species and the environmental dissolved Fe concentration (Kulkarni et al., 2006; Sunda and Huntsman,  
719 1995; King et al., 2012; Boyd et al., 2015). In our results the Fe:POC values ranged from 1200 to 39 000  $\mu\text{mol mol}^{-1}$ , which  
720 may be due to the particulate trace metal richness of the Derwent Estuary (control) and/or the addition of lithogenic particles  
721 (slag and olivine treatment). The presence of abiotic particulate metal sources creates challenges to quantify metal quotas  
722 and then to evaluate metal accumulation effects on biological organisms.

723

724 Our study reveals that the added minerals enriched the particulate trace metal pools to various degrees. Consistent with the  
725 dissolved trace metal data, the slag treatment was enriched with particulate Fe and Mn while the olivine treatment was  
726 enriched with particulate Fe and Ni. The enhanced particulate Ni and Mn concentrations were higher than before mineral  
727 additions and the control levels. This is in line with previous research which indicates a positive correlation between  
728 particulate and dissolved trace metal concentrations (Gaulier et al., 2019).

729

730 Based on the amounts released through OAE as simulated herein, it appears that Ni and Mn have the highest potential to  
731 cause toxicity in certain marine organisms (Jakimska et al., 2011). These trace metals have the potential to accumulate in  
732 marine organisms over time (bioaccumulation effects), and their increased concentrations in the food chain can lead to  
733 adverse effects on the health and well-being of organisms at higher trophic levels (biomagnification effects). One crucial  
734 next step will be to investigate whether the enhanced dissolved/particulate trace metal will affect higher trophic levels to  
735 estimate the environmental risks of OAE on other marine organisms.

736

## 737 **5 Conclusions**

738 Our study aimed to assess the environmental impacts of two ground OAE minerals, olivine and steel slag, on coastal  
739 plankton communities. Both minerals released alkalinity, leading to an elevation in  $\text{pH}_T$ . However, the addition of steel  
740 slag exhibited significantly higher efficiency in elevating alkalinity compared to olivine.

741

742 Approximately  $1.9 \text{ g L}^{-1}$  of olivine powder were added in the olivine treatments, leading to a  $29 \mu\text{mol kg}^{-1}$  increase in  
743 alkalinity and increased concentrations of  $\text{Si(OH)}_4$  and trace metals (Fe and Ni). Compared to this relatively modest  
744 increase of alkalinity and associated  $\text{CO}_2$  removal potential, the impacts on the plankton community appeared to be  
745 relatively pronounced. Thus, although our experiment ran for only 3 weeks, and olivine powder may slowly release more  
746 alkalinity, the short-term response monitored here suggests that the immediate climatic benefit is relatively small compared  
747 to a relatively pronounced environmental effect.

748

749 Only  $0.038 \text{ g L}^{-1}$  of slag were added to the treatment but this led to an alkalinity enhancement of  $361 \mu\text{mol kg}^{-1}$  and the  
750 increased concentrations of macronutrients (P and Si) and trace metals (Mn and Fe) additions as well as changes in  
751 carbonate chemistry. Although limited environmental impacts were observed from the slag treatment in our experiment,  
752 some aspects require further study. For example, the pronounced release of P could cause eutrophication and the relatively  
753 rapid increase in pH may be a detrimental aspect if organisms cannot acclimate fast enough. Furthermore, it is essential to  
754 consider that the composition of steel slag can vary depending on the source factory (Wang et al., 2011; Proctor et al.,  
755 2000), which may affect the efficiency of carbon removal and change the trace metal perturbation. Nevertheless, just based  
756 on our experiment, the comparison between the immediate climatic benefit and environmental effect appears to be more  
757 favourable for slag than olivine.

758

759 Based on our findings, it can be concluded that steel slag powder exhibited fewer environmental impacts on plankton  
760 communities compared to olivine powder relative to its capacity for alkalinity enhancement. The results highlight the

761 importance of carefully assessing the environmental consequences of using specific OAE minerals, particularly when  
762 considering their potential effects on plankton communities.

763

764 **Data availability.** Data are available in the Institute for Marine and Antarctic Studies (IMAS) data catalogue, University  
765 of Tasmania (UTAS) (<https://doi.org/10.25959/X6FH-9K15>, Guo, J., & Bach, L. (2023)).

766

767 **Author contributions.** LTB, RFS, KMS and JAG designed the experiments and JAG carried them out. LTB, RFS and  
768 KMS supervised the study. ATT analysed the dissolved/particulate trace metal samples. JAG conducted statistical analyses.  
769 JAG prepared the manuscript with contributions from all authors.

770

771 **Competing interests.** The contact author has declared that none of the authors has any competing interests.

772

773 **Disclaimer.** Publisher's note: Copernicus Publications remains neutral with regard to jurisdictional claims in published  
774 maps and institutional affiliations.

775

776 **Acknowledgements.** We would like to thank Steve Van Orsouw from Moyne Shire Council, Victoria, Australia for  
777 providing olivine rocks. We also thank Bradley Mansell who provided the Basic Oxygen Slag from Liberty Primary Steel  
778 Whyalla Steelworks in Whyalla, South Australia, Australia. We thank Sandrin Feig and Thomas Rodemann for their support  
779 on scanning electron microscopy and particulate organic matter. We appreciate the assistance of Pam Quayle and Axel  
780 Durand (IMAS) in the lab, particularly with particulate metal digestions.

781

782 **Financial support.** This research has been supported by the Australian Research Council through a Future Fellowship  
783 project (FT200100846 to LTB), the Carbon to Sea Initiative (LTB), and by the Australian Antarctic Program Partnership  
784 (ASCI000002 to RFS, KMS and JAG). Access to SF-ICP-MS instrumentation was facilitated through ARC LIEF funding  
785 (LE0989539) awarded to ATT. JAG thanks the Australian Research Training Program (RTP) for her scholarship.

## 786 **References**

- 787 Ackerman, L., Jelínek, E., Medaris, G., Ježek, J., Siebel, W., and Strnad, L.: Geochemistry of Fe-rich peridotites and  
788 associated pyroxenites from Horní Bory, Bohemian Massif: Insights into subduction-related melt–rock reactions,  
789 *Chem. Geol.*, 259, 152-167, <https://doi.org/10.1016/j.chemgeo.2008.10.042>, 2009.
- 790 Al-Azri, A., Al-Hashmi, K., Goes, J., Gomes, H., Rushdi, A. I., Al-Habsi, H., Al-Khusaibi, S., Al-Kindi, R., and Al-Azri, N.:  
791 Seasonality of the bloom-forming heterotrophic dinoflagellate *Noctiluca scintillans* in the Gulf of Oman in relation  
792 to environmental conditions, *Int. J. Oceans Oceanogr.*, 2, 51-60, 2007.
- 793 Armstrong, F. A.: Why did nature choose manganese to make oxygen?, *Philos Trans R Soc Lond B Biol Sci*, 363, 1263-1270,  
794 <https://doi.org/10.1098/rstb.2007.2223>, 2008.
- 795 Bach, L. T., Gill, S. J., Rickaby, R. E. M., Gore, S., and Renforth, P.: CO2 removal with enhanced weathering and ocean  
796 alkalinity enhancement: potential risks and co-benefits for marine pelagic ecosystems, *Front Clim*, 1, 1-21,  
797 <http://doi.org/10.3389/fclim.2019.00007>, 2019.
- 798 Balaguer, J., Koch, F., Hassler, C. et al.: Iron and manganese co-limit the growth of two phytoplankton groups dominant at  
799 two locations of the Drake Passage. *Commun Biol* 5, 207, <https://doi.org/10.1038/s42003-022-03148-8>, 2022.
- 800 Baliarsingh, S. K., Lotliker, A. A., Trainer, V. L., Wells, M. L., Parida, C., Sahu, B. K., Srichandan, S., Sahoo, S., Sahu, K. C., and  
801 Kumar, T. S.: Environmental dynamics of red *Noctiluca scintillans* bloom in tropical coastal waters, *Mar. Pollut. Bull.*,  
802 111, 277-286, <https://doi.org/10.1016/j.marpolbul.2016.06.103>, 2016.
- 803 Basu, S. and Mackey, K. R. M.: Phytoplankton as key mediators of the biological carbon pump: their responses to a



804 changing climate, *Sustainability*, 10, 869, <https://doi.org/10.3390/su10030869>, 2018.

805 Behrenfeld, M. J., Worthington, K., Sherrell, R. M., Chavez, F. P., Strutton, P., McPhaden, M., and Shea, D. M.: Controls on  
806 tropical Pacific Ocean productivity revealed through nutrient stress diagnostics, *Nature*, 442, 1025-1028,  
807 <https://doi.org/10.1038/nature05083>, 2006.

808 Bowie, A. R., Townsend, A. T., Lannuzel, D., Remenyi, T. A., and van der Merwe, P.: Modern sampling and analytical  
809 methods for the determination of trace elements in marine particulate material using magnetic sector inductively  
810 coupled plasma-mass spectrometry, *Anal Chim Acta*, 676, 15-27, <https://doi.org/10.1016/j.aca.2010.07.037>, 2010.

811 Boyd, P. W., Strzepek, R. F., Ellwood, M. J., Hutchins, D. A., Nodder, S. D., Twining, B. S., and Wilhelm, S. W.: Why are biotic  
812 iron pools uniform across high- and low-iron pelagic ecosystems?, *Global Biogeochem. Cycles*, 29, 1028-1043,  
813 <http://doi.org/10.1002/2014gb005014>, 2015.

814 Boyd, P. W., Jickells, T., Law, C., Blain, S., Boyle, E., Buesseler, K., Coale, K., Cullen, J., De Baar, H. J., and Follows, M.:  
815 Mesoscale iron enrichment experiments 1993-2005: synthesis and future directions, *Science*, 315, 612-617,  
816 <http://doi.org/10.1126/science.1131669>, 2007.

817 Bruland, K. W. and Lohan, M. C.: 6.02 Controls of Trace Metals in Seawater, in: *Treatise on Geochemistry*, edited by:  
818 Elderfield, H., Holland, H. D., and Turekian, K. K., Elsevier Pergamon, 23-47, [http://doi.org/10.1016/b0-08-043751-](http://doi.org/10.1016/b0-08-043751-6/06105-3)  
819 [6/06105-3](http://doi.org/10.1016/b0-08-043751-6/06105-3), 2003.

820 Burt, D. J., Fröb, F., and Ilyina, T.: The sensitivity of the marine carbonate system to regional ocean alkalinity enhancement,  
821 *Front Clim*, 3, <http://doi.org/10.3389/fclim.2021.624075>, 2021.

822 Caserini, S., Storni, N., and Grosso, M.: The availability of limestone and other raw materials for ocean alkalinity  
823 enhancement, *Global Biogeochem. Cycles*, 36, <http://doi.org/10.1029/2021gb007246>, 2022.

824 De Baar, H. J., Boyd, P. W., Coale, K. H., Landry, M. R., Tsuda, A., Assmy, P., Bakker, D. C., Bozec, Y., Barber, R. T., and Brzezinski,  
825 M. A.: Synthesis of iron fertilization experiments: from the iron age in the age of enlightenment, *J Geophys Res*  
826 *Oceans*, 110, <https://doi.org/10.1029/2004JC002601>, 2005.

827 Dickson, A. G., Sabine, C. L., and Christian, J. R.: Guide to best practices for ocean CO<sub>2</sub> measurements, North Pacific Marine  
828 Science Organization, Canada2007.

829 Egge, J. and Jacobsen, A.: Influence of silicate on particulate carbon production in phytoplankton, *Mar. Ecol. Prog. Ser.*,  
830 147, 219-230, <http://doi.org/10.3354/meps147219>, 1997.

831 Evans, C., O'Reilly, J. E., and Thomas, J.: A handbook for the measurement of chlorophyll and primary production, 1987.

832 Falkowski, P. G.: The role of phytoplankton photosynthesis in global biogeochemical cycles, *Photosynthesis Research*, 39,  
833 235-258, <https://doi.org/10.1007/BF00014586>, 1994.

834 Feng, E. Y., Koeve, W., Keller, D. P., and Oschlies, A.: Model-based assessment of the CO<sub>2</sub> sequestration potential of coastal  
835 ocean alkalization, *Earth's Future*, 5, 1252-1266, <http://doi.org/10.1002/2017ef000659>, 2017.

836 Ferderer, A., Chase, Z., Kennedy, F., Schulz, K. G., and Bach, L. T.: Assessing the influence of ocean alkalinity enhancement  
837 on a coastal phytoplankton community, *Biogeosciences*, 19, 5375-5399, <http://doi.org/10.5194/bg-19-5375-2022>,  
838 2022.

839 Ferderer, A., Schulz, K. G., Riebesell, U., Baker, K. G., Chase, Z., and Bach, L. T.: Investigating the effect of silicate and calcium  
840 based ocean alkalinity enhancement on diatom silicification, *Biogeosciences Discuss.* [preprint],  
841 <https://doi.org/10.5194/bg-2023-144>, in review, 2023.

842 Package 'seacarb'-Seawater Carbonate Chemistry: <https://cran.r-project.org/web/packages/seacarb/index.html>, last  
843 access: 2023/6/1.

844 Gaulier, C., Zhou, C., Guo, W., Bratkic, A., Superville, P. J., Billon, G., Baeyens, W., and Gao, Y.: Trace metal speciation in  
845 North Sea coastal waters, *Sci. Total Environ.*, 692, 701-712, <http://doi.org/10.1016/j.scitotenv.2019.07.314>, 2019.

846 Guo, J., Bao, Y., and Wang, M.: Steel slag in China: Treatment, recycling, and management, *Waste Management*, 78, 318-  
847 330, <https://doi.org/10.1016/j.wasman.2018.04.045>, 2018.

848 Guo, J. A., Strzepek, R., Willis, A., Ferderer, A., and Bach, L. T.: Investigating the effect of nickel concentration on  
849 phytoplankton growth to assess potential side-effects of ocean alkalinity enhancement, *Biogeosciences*, 19, 3683-  
850 3697, <https://doi.org/10.5194/bg-19-3683-2022>, 2022.

851 Hallegraeff, G. M., Albinsson, M. E., Dowdney, J., Holmes, A. K., Mansour, M. P., and Seger, A.: Prey preference,  
852 environmental tolerances and ichthyotoxicity by the red-tide dinoflagellate *Noctiluca scintillans* cultured from  
853 Tasmanian waters, *J. Plankton Res.*, 41, 407-418, <https://doi.org/10.1093/plankt/fbz037>, 2019.

854 Hansen, H. P. and Koroleff, F.: Determination of nutrients, in: *Methods of seawater analysis*, edited by: Grasshoff, K.,  
855 Kremling, K., and Ehrhardt, M., 159-228, <https://doi.org/10.1002/9783527613984.ch10>, 1999.

856 Hartmann, J., West, A. J., Renforth, P., Köhler, P., De La Rocha, C. L., Wolf-Gladrow, D. A., Dürr, H. H., and Scheffran, J.:  
857 Enhanced chemical weathering as a geoengineering strategy to reduce atmospheric carbon dioxide, supply  
858 nutrients, and mitigate ocean acidification, *Rev. Geophys.*, 51, 113-149, <http://doi.org/10.1002/rog.20004>, 2013.

859 Humphreys, M. P., Lewis, E. R., Sharp, J. D., and Pierrot, D.: PyCO<sub>2</sub>SYs v1. 8: marine carbonate system calculations in  
860 Python, *Geosci Model Dev*, 15, 15-43, <https://doi.org/10.5194/gmd-15-15-2022>, 2022.

861 Hutchins, D. A., Fu, F.-X., Yang, S.-C., John, S. G., Romaniello, S. J., Andrews, M. G., and Walworth, N. G.: Responses of  
862 globally important phytoplankton species to olivine dissolution products and implications for carbon dioxide  
863 removal via ocean alkalinity enhancement, *Biogeosciences*, 20, 4669–4682, [https://doi.org/10.5194/bg-20-4669-](https://doi.org/10.5194/bg-20-4669-2023)  
864 2023, 2023.

865 Ilyina, T., Wolf-Gladrow, D., Munhoven, G., and Heinze, C.: Assessing the potential of calcium-based artificial ocean  
866 alkalinization to mitigate rising atmospheric CO<sub>2</sub> and ocean acidification, *Geophys. Res. Lett.*, 40, 5909-5914,  
867 <https://doi.org/10.1002/2013GL057981>, 2013.

868 Jakimska, A., Konieczka, P., Skóra, K., and Namieśnik, J.: Bioaccumulation of metals in tissues of marine animals, Part II:  
869 metal concentrations in animal tissues, *Pol J Environ Stud*, 20, 2011.

870 Keller, D. P., Feng, E. Y., and Oschlies, A.: Potential climate engineering effectiveness and side effects during a high carbon  
871 dioxide-emission scenario, *Nat. Commun.*, 5, 3304, <https://doi.org/10.1038/ncomms4304>, 2014.

872 King, A. L., Sañudo-Wilhelmy, S. A., Boyd, P. W., Twining, B. S., Wilhelm, S. W., Breene, C., Ellwood, M. J., and Hutchins, D.  
873 A.: A comparison of biogenic iron quotas during a diatom spring bloom using multiple approaches, *Biogeosciences*,  
874 9, 667-687, <http://doi.org/10.5194/bg-9-667-2012>, 2012.

875 Kohler, P., Hartmann, J., and Wolf-Gladrow, D. A.: Geoengineering potential of artificially enhanced silicate weathering of  
876 olivine, *Proc. Natl. Acad. Sci. USA*, 107, 20228-20233, <https://doi.org/10.1073/pnas.1000545107>, 2010.

877 Kourounis, S., Tsvilis, S., Tsakiridis, P. E., Papadimitriou, G. D., and Tsibouki, Z.: Properties and hydration of blended  
878 cements with steelmaking slag, *Cem. Concr. Res.*, 37, 815-822, <https://doi.org/10.1016/j.cemconres.2007.03.008>,  
879 2007.

880 Kulkarni, P. P., She, Y. M., Smith, S. D., Roberts, E. A., and Sarkar, B.: Proteomics of metal transport and metal-associated  
881 diseases, *Chemistry*, 12, 2410-2422, <http://doi.org/10.1002/chem.200500664>, 2006.

882 Lenton, A., Matear, R. J., Keller, D. P., Scott, V., and Vaughan, N. E.: Assessing carbon dioxide removal through global and  
883 regional ocean alkalinization under high and low emission pathways, *Earth. Syst. Dyn.*, 9, 339-357,  
884 <https://doi.org/10.5194/esd-9-339-2018>, 2018.

885 Lombard, F., Selander, E., and Kjørboe, T.: Active prey rejection in the filter-feeding appendicularian *Oikopleura dioica*,  
886 *Limnol. Oceanogr.*, 56, 1504-1512, <http://doi.org/10.4319/lo.2011.56.4.1504>, 2011.

887 Lueker, T. J., Dickson, A. G., and Keeling, C. D.: Ocean pCO<sub>2</sub> calculated from dissolved inorganic carbon, alkalinity, and  
888 equations for K<sub>1</sub> and K<sub>2</sub>: validation based on laboratory measurements of CO<sub>2</sub> in gas and seawater at equilibrium,  
889 *Mar. Chem.*, 70, 105-119, [https://doi.org/10.1016/S0304-4203\(00\)00022-0](https://doi.org/10.1016/S0304-4203(00)00022-0), 2000.

890 Macleod, C. and Coughanowr, C.: Heavy metal pollution in the Derwent estuary: History, science and management, *Reg.*  
891 *Stud. Mar. Sci.*, 32, <http://doi.org/10.1016/j.rsma.2019.100866>, 2019.

892 Moore, C. M., Mills, M. M., Arrigo, K. R., Berman-Frank, I., Bopp, L., Boyd, P. W., Galbraith, E. D., Geider, R. J., Guieu, C.,  
893 Jaccard, S. L., Jickells, T. D., La Roche, J., Lenton, T. M., Mahowald, N. M., Marañón, E., Marinov, I., Moore, J. K.,  
894 Nakatsuka, T., Oschlies, A., Saito, M. A., Thingstad, T. F., Tsuda, A., and Ulloa, O.: Processes and patterns of oceanic  
895 nutrient limitation, *Nat. Geosci.*, 6, 701-710, <http://doi.org/10.1038/ngeo1765>, 2013.

896 Nelson, D. M., Smith Jr, W. O., Muench, R. D., Gordon, L. I., Sullivan, C. W., and Husby, D. M.: Particulate matter and nutrient  
897 distributions in the ice-edge zone of the Weddell Sea: relationship to hydrography during late summer, *Deep. Sea.*  
898 *Res. A*, 36, 191-209, [https://doi.org/10.1016/0198-0149\(89\)90133-7](https://doi.org/10.1016/0198-0149(89)90133-7), 1989.

899 NRMCC, N. a.: The Australian Drinking Water Guidelines (2011) - Version 3.8 Updated 2022, 2022.

900 Pausch, F., Bischof, K., Trimborn, S.: Iron and manganese co-limit growth of the Southern Ocean diatom *Chaetoceros debilis*.  
901 *PLOS ONE* 14, e0221959.. <https://doi.org/10.1371/journal.pone.0221959>, 2019.

902 Paquay, F. S. and Zeebe, R. E.: Assessing possible consequences of ocean liming on ocean pH, atmospheric CO<sub>2</sub>  
903 concentration and associated costs, *Int. J. Greenh. Gas Control.*, 17, 183-188,  
904 <https://doi.org/10.1016/j.ijggc.2013.05.005>, 2013.

905 Platt, T., Gallegos, C. L., and Harrison, W. G.: Photoinhibition of photosynthesis in natural assemblages of marine  
906 phytoplankton, *J. Mar. Res.*, 38, 687-701, 1980.

907 Proctor, D. M., Fehling, K. A., Shay, E. C., Wittenborn, J. L., Green, J. J., Avent, C., Bigham, R. D., Connolly, M., Lee, B.,  
908 Shepker, T. O., and Zak, M. A.: Physical and chemical characteristics of blast furnace, basic oxygen furnace, and  
909 electric arc furnace steel industry slags, *Environ. Sci. Technol.*, 34, 1576-1582, <http://doi.org/10.1021/es9906002>,  
910 2000.

911 Reichl, C., Schatz, M., and Zsak, G.: World mining data, 1-261, 2018.

912 Renforth, P.: The negative emission potential of alkaline materials, *Nat. Commun.*, 10, [http://doi.org/10.1038/s41467-](http://doi.org/10.1038/s41467-019-09475-5)  
913 019-09475-5, 2019.

914 Renforth, P. and Henderson, G.: Assessing ocean alkalinity for carbon sequestration, *Rev. Geophys.*, 55, 636-674,  
915 <http://doi.org/10.1002/2016rg000533>, 2017.

916 Schallenberg, C., Strzepek, R. F., Schuback, N., Clementson, L. A., Boyd, P. W., and Trull, T. W.: Diel quenching of Southern  
917 Ocean phytoplankton fluorescence is related to iron limitation, *Biogeosciences*, 17, 793-812,

918 <https://doi.org/10.5194/bg-17-793-2020>, 2020.

919 Schuiling, R. D. and Krijgsman, P.: Enhanced weathering: an effective and cheap tool to sequester CO<sub>2</sub>, *Clim. Change*, 74,  
920 349-354, <https://doi.org/10.1007/s10584-005-3485-y>, 2006.

921 Selfe, C.: Developing Transfer Function to Measuring Phytoplankton Cellular Properties with Flow Cytometry, Master's  
922 thesis, Institute of Marine and Antarctic Studies, University of Tasmania, Australia, 2022.

923 Comparing smooths in factor-smooth interactions II ordered factors:  
924 <https://fromthebottomoftheheap.net/2017/12/14/difference-splines-ii/>, last access: March 2023.

925 Smith, S. M., Geden, O., Nemet, G. F., Gidden, M. J., Lamb, W. F., Powis, C., Bellamy, R., Callaghan, M. W., Cowie, A., Cox,  
926 E., Fuss, S., Gasser, T., Grassi, G., Greene, J., Lück, S., Mohan, A., Müller-Hansen, F., Peters, G. P., Pratama, Y., Repke,  
927 T., Riahi, K., Schenuit, F., Steinhauser, J., Streffler, J., Valenzuela, J. M., and Minx, J. C.: The State of Carbon Dioxide  
928 Removal - 1st Edition, <http://doi.org/10.17605/OSF.IO/W3B4Z>, 2023.

929 Sohrin, Y. and Bruland, K. W.: Global status of trace elements in the ocean, *TrAC, Trends Anal. Chem.*, 30, 1291-1307,  
930 <https://doi.org/10.1016/j.trac.2011.03.006>, 2011.

931 Strzeppek, R. F. and Harrison, P. J.: Photosynthetic architecture differs in coastal and oceanic diatoms, *Nature*, 431, 689-  
932 692, <http://doi.org/10.1038/nature02954>, 2004.

933 Su, B., Chen, Y., Guo, S., and Liu, J.: Origins of orogenic dunites: petrology, geochemistry, and implications, *Gondwana Res.*,  
934 29, 41-59, <https://doi.org/10.1016/j.gr.2015.08.001>, 2016.

935 Subhas, A. V., Marx, L., Reynolds, S., Flohr, A., Mawji, E. W., Brown, P. J., and Cael, B.: Microbial ecosystem responses to  
936 alkalinity enhancement in the North Atlantic Subtropical Gyre, *Front Clim*, 4,  
937 <https://doi.org/10.3389/fclim.2022.784997>, 2022.

938 Sunda, W. G.: Trace metal-phytoplankton interactions in aquatic systems, in: *Environmental Microbe-Metal Interactions*,  
939 edited by: Lovley, D. R., 79-107, <https://doi.org/10.1128/9781555818098.ch4>, 2000.

940 Sunda, W. G.: Feedback interactions between trace metal nutrients and phytoplankton in the ocean, *Frontiers in*  
941 *Microbiology*, 3, 1-22, <http://doi.org/10.3389/fmicb.2012.00204>, 2012.

942 Sunda, W. G. and Huntsman, S. A.: Iron Uptake and Growth Limitation in Oceanic and Coastal Phytoplankton, *Marine*  
943 *Chemistry*, 50, 189-206, Doi 10.1016/0304-4203(95)00035-P, 1995.

944 Sunda, W. G. and Huntsman, S. A.: Interrelated influence of iron, light and cell size on marine phytoplankton growth,  
945 *Nature*, 390, 389-392, <http://doi.org/10.1038/37093>, 1997.

946 Tang, D. G. and Morel, F. M. M.: Distinguishing between cellular and Fe-oxide-associated trace elements in phytoplankton,  
947 *Mar. Chem.*, 98, 18-30, <http://doi.org/10.1016/j.marchem.2005.06.003>, 2006.

948 Tovar-Sanchez, A., Sanudo-Wilhelmy, S. A., Garcia-Vargas M., Weaver R. S., Popels L., C., and Hutchins D. A.: A trace metal  
949 clean reagent to remove surface-bound iron from marine phytoplankton. *Mar. Chem.*, 82, 1-2, 91-99,  
950 [https://doi.org/10.1016/S0304-4203\(03\)00054-9](https://doi.org/10.1016/S0304-4203(03)00054-9), 2003.

951 Twining, B. S. and Baines, S. B.: The trace metal composition of marine phytoplankton, *Ann. Rev. Mar. Sci.*, 5, 191-215,  
952 <http://doi.org/10.1146/annurev-marine-121211-172322>, 2013.

953 Wafar, M., Le Corre, P., and L'Helguen, S.: f-Ratios calculated with and without urea uptake in nitrogen uptake by  
954 phytoplankton, *Deep Sea Res. I Oceanogr. Res. Pap.*, 42, 1669-1674, [https://doi.org/10.1016/0967-0637\(95\)00066-F](https://doi.org/10.1016/0967-0637(95)00066-F), 1995.

956 Wang, Q., Yan, P., and Feng, J.: A discussion on improving hydration activity of steel slag by altering its mineral  
957 compositions, *J. Hazard. Mater.*, 186, 1070-1075, <https://doi.org/10.1016/j.jhazmat.2010.11.109>, 2011.

958 Wang, W.: Interactions of trace metals and different marine food chains, *Mar. Ecol. Prog. Ser.*, 243, 295-309,  
959 <http://doi.org/10.3354/meps243295>, 2002.

960 Wolfe-Simon, F., Grzebyk, D., Schofield, O., and Falkowski, P. G.: The role and evolution of superoxide dismutases in algae,  
961 *J. Phycol.*, 41, 453-465, <https://doi.org/10.1111/j.1529-8817.2005.00086.x>, 2005.

962 Xin, X., Faucher, G., and Riebesell, U.: Phytoplankton response to Increased nickel in the context of ocean alkalinity  
963 enhancement, *Biogeosciences* [preprint], <https://doi.org/10.5194/bg-2023-130>, 2023.

964 Zhang, W., Dong, Z., Zhang, C., Sun, X., Hou, C., Liu, Y., Wang, L., Ma, Y., and Zhao, J.: Effects of physical-biochemical  
965 coupling processes on the *Noctiluca scintillans* and *Mesodinium* red tides in October 2019 in the Yantai nearshore,  
966 China, *Mar. Pollut. Bull.*, 160, 111609, <https://doi.org/10.1016/j.marpolbul.2020.111609>, 2020.

967